

Critical Evaluation of Studies Alleging Evidence for Technosignatures in the POSS1-E Photographic Plates

WESLEY ANDRÉS WATTERS,¹ LAURA DOMINÉ,² SARAH LITTLE,³ CAMERON PRATT,³ AND KEVIN H. KNUTH⁴

¹ *Whitin Observatory, Dept. Physics and Astronomy, Wellesley College*

² *National Institute of Information and Communications Technology (NICT), Koganei, Tokyo, Japan*

³ *Scientific Coalition for UAP Studies, Fort Myers, FL*

⁴ *Department of Physics, State University of New York at Albany*

ABSTRACT

Recent studies by B. Villarroel and colleagues have assembled and analyzed datasets of unidentified features measured from digital scans of photographic plates captured by the first-epoch Palomar Observatory Sky Survey (POSS1) in the pre-Sputnik era. These studies have called attention to (i) a purported deficit of features within Earth's shadow; (ii) the sporadic presence of linear clusters; and (iii) a positive correlation between the timing of feature observations and nuclear tests as well as Unidentified Aerial Phenomena (UAP) sighting reports. These observations were cited as evidence that some fraction of the unidentified features represent glinting artificial objects near Earth. We have examined these claims using two related, previously published datasets. When analyzing the most vetted of these, we do not observe the reported deficit in the terrestrial shadow. We determine that a third of the features in the reported linear clusters were not confidently distinguished from catalog stars. We find that the reported correlation between the timing of feature observations and nuclear tests becomes insignificant after properly normalizing by the number of observation days, and is almost completely determined by the observation schedule of the Palomar telescope. We uncover important inconsistencies in the definitions of the datasets used in these studies, as well as the use of unvalidated datasets containing catalog stars, scan artifacts, and plate defects. It has not been shown that any of the features in these datasets represent optical transients. We examine the spatial distribution of the plate-derived features, finding an overall gradual increase in number density toward the corners and edges of plates, as well as examples of (i) empty north-south strips that span multiple plates; (ii) clusters and voids having geometric shapes; and (iii) amorphous clusters. We also highlight a circular argument used in these studies, that leverages the consequences of hypotheses about the origins of the plate-derived features to justify confidence in the validity of the measurements. Finally, we also review the literature concerning historical searches for optical transients in photographic plates corresponding to gamma ray bursts (GRBs); following decades of work, researchers were unable to make a confident identification of a GRB-associated optical transient.

Keywords: UAP, SETI, optical transients, technosignatures

1. INTRODUCTION

In the past five years, the study of Unidentified Aerial Phenomena or Unidentified Anomalous Phenomena (UAP) has been acknowledged as an important scientific endeavor by several teams of academic scientists (H. Kayal 2022; G. P. Nolan et al. 2022; A. A. Loeb & F. H. Laukien 2023; W. A. Watters et al. 2023; M. Szydagis et al. 2025) and by a NASA-commissioned re-

port (NASA 2023). This recent work has built upon decades of prior scholarship and investigation by other academic scientists, government groups, and private research organizations (P. Ailleris 2011, 2024; K. H. Knuth et al. 2025). It has been understood for decades that the vast majority of sighting reports (95-99%) implicate known objects and phenomena. A stubborn residuum has resisted conventional explanation (J. A. Hynek 1966; J. E. McDonald 1972; K. H. Knuth et al. 2025). This has inspired some scientists to investigate these phenomena using modern statistical methods, machine learn-

ing, and specially-designed scientific instrumentation, while suspending judgment about their ultimate origin (e.g., M. Teodorani 2004; W. A. Watters et al. 2023; L. Dominé et al. 2025; M. Szydagis et al. 2025). In parallel, a subset of researchers engaged in the Search for Extraterrestrial Intelligence (SETI) has proposed searching for novel technosignatures within the Solar System (J. Haqq-Misra & R. K. Kopparapu 2012; S. Shostak 2020; B. Villarroel et al. 2025b). Many scientists participating in this new wave of research have stressed the importance of (i) imposing rigorous evidential standards, (ii) using calibrated instrumentation, (iii) investigating and completely understanding sources of error, and (iv) ensuring proper data validation (e.g., W. A. Watters et al. 2023; M. Lingam et al. 2023; L. Dominé et al. 2025; M. Szydagis et al. 2025).

B. Villarroel et al. (2021, 2022) described searches in astronomical data records from the pre-Sputnik era for local technosignatures in the form of glinting artificial satellites. In the present study, we perform a critical examination of the data, analyses, and results presented in recent papers by B. Villarroel et al. (2025c) and S. Bruehl & B. Villarroel (2025) that build on this previous work. Both papers use datasets of nominally unidentified features that derive from datasets generated by E. Solano et al. (2022) using two sets of complete digital scans of the first-epoch Palomar Observatory Sky Survey (POSS1, 1949-1957): (i) the Space Telescope Science Institute’s Digital Sky Survey⁵ (DSS) and (ii) the SuperCOSMOS survey (N. C. Hambly et al. 2001). The first paper (B. Villarroel et al. 2025c) suggests that some fraction of the features may represent objects reflecting sunlight in near-Earth space. This conclusion is heavily based on an alleged deficit of features in the Earth’s shadow. Previous work was also concerned with the search for statistically significant alignments and clusters of the purportedly unidentified POSS1 features (E. Solano et al. 2024; B. Villarroel et al. 2021, 2022). The second study (S. Bruehl & B. Villarroel 2025) reports a correlation between the days when features were recorded and the timing of nuclear weapons tests as well as when UAP sightings were reported.

We shall use the term “Selected POSS1-E features” (SPFs) to refer to features selected from POSS1-E plates in these and other studies, where the selection criteria differed depending on the dataset in question. We have done this partly in order to suspend judgment about the ultimate origin(s) of the features studied in B. Villarroel et al. (2025c) and E. Solano et al. (2022). In the present

study, we examine three publicly available datasets of SPFs. Two of these were catalogued in E. Solano et al. (2022), and derive from the same parent dataset as the subsets analyzed in S. Bruehl & B. Villarroel (2025) and B. Villarroel et al. (2025c). For purposes of comparison, we also make use of a dataset of SPFs that appear in both the POSS1-E (red band) and POSS1-O (blue band) plates, which are hence likely of celestial origin. This third dataset was sampled as part of an independent study by the Minnesota Automated Plate Scanner (MAPS) project (R. L. Pennington et al. 1993; J. E. Cabanella et al. 2003). We also use these datasets, along with information in S. Bruehl & B. Villarroel (2025) and B. Villarroel et al. (2025c), to describe the datasets addressed in those studies. Access to the contents of these latter datasets is not necessary to derive our conclusions.

Regarding the SPFs used in B. Villarroel et al. (2025c) and S. Bruehl & B. Villarroel (2025) to estimate correlations with the terrestrial shadow and nuclear tests, our work suggests that (i) a significant fraction (at least 91%) of these were part of a set removed by E. Solano et al. (2022) for residing within 5'' of catalog stars; (ii) a potentially significant but undetermined amount are at risk of being star-like plate emulsion artifacts; and (iii) up to 40% are at risk of being scan artifacts of the type removed by E. Solano et al. (2022) to obtain their most vetted dataset. B. Villarroel et al. (2025c) acknowledged⁶ the possibility that a significant fraction of SPFs in the analyzed datasets are the result of emulsion defects, degradation, and contamination, and did not formally validate these datasets in order to rule this out.

In Section 2, we briefly review the literature about a two-decade search in archival plates for then-novel optical transients related to gamma ray bursts (GRBs), which revealed common star-like emulsion defects and the difficulties in distinguishing these from optical flashes. In Section 3, we define and describe the datasets under consideration while pointing out significant ambiguities and inconsistencies, as well as caveats associated with their principal uses in B. Villarroel et al. (2025c) and S. Bruehl & B. Villarroel (2025). Section 4 addresses the spatial distribution of SPFs between plates, within plates, and across the sky, suggesting plate artifacts as their likely origin. We also examine the SPFs reported to occur within sporadic linear clusters in B. Villarroel et al. (2025c), finding that a third of these

⁵ <https://archive.stsci.edu/dss/acknowledging.html>

⁶ e.g., See Section 8, pg 16 of B. Villarroel et al. (2025c): “this sample... is expected to contain a substantial number of false positives, including clustered artifacts such as edge fingerprints or other plate defects that contaminate our sample.”

were discarded by E. Solano et al. (2022). Section 5 critically examines the purported deficit of SPF in Earth's shadow reported in B. Villarroel et al. (2025c) and offered as evidence that these represent glinting artificial satellites in the pre-Sputnik era. Using the most vetted dataset in E. Solano et al. (2022), we find no evidence of a deficit. Section 6 addresses the alleged correlation between SPF and the timing of nuclear tests as reported in S. Bruehl & B. Villarroel (2025), finding that this correlation is almost entirely determined by the Palomar telescope observation schedule. The discussion in Section 7 focuses on major challenges to the analyses and conclusions in both of the studies we have examined, including the description a circular argument used to justify confidence in the conclusions as well as the validity of measurements.

2. HISTORICAL SEARCHES FOR OPTICAL TRANSIENTS IN PHOTOGRAPHIC PLATES

B. Villarroel et al. (2025c) and S. Bruehl & B. Villarroel (2025) analyzed SPF datasets that we describe in Section 3 and were motivated by questions developed in E. Solano et al. (2022), E. Solano et al. (2024), B. Villarroel et al. (2021) and B. Villarroel et al. (2022). The goal of their work is to uncover evidence of technosignatures in the form of unidentified optical transients in pre-Sputnik photographic plates acquired by the National Geographic POSS1 survey (R. L. Minkowski & G. O. Abell 1963). The validity of this entire body of work rests on the premise that the selected features are in fact images of real optical transients distinct from stars and other celestial bodies, and are not plate artifacts or other defects of spurious origin unrelated to objects in the sky.

The confident identification of optical transients (short-lived optical emissions) in archival photographic plates was the goal of a two-decade-long effort to identify the first optical flash counterpart of a gamma-ray burst (GRB). GRB optical counterparts were postulated as a new and unproven source of optical transients (OTs), similar to the role played by non-anthropogenic technosignatures in the work of Villarroel and colleagues, except that the GRBs were an independently verified phenomenon with estimates of position in the sky. Work began in 1974 (J. Grindlay et al. 1974), but the first gamma-ray OT candidate was announced in 1981 after searching 4,135 physical plates from Harvard University Observatory spanning 1889-1953 and 1970-1979 (B. E. Schaefer 1981). Researchers then combed the physical plate collections of the Harvard, Sonneberg, Ondfejov, and Bamberg observatories (~910,000 plates; R. Hudec et al. (1994)) and attempted to determine if any of the

transient, star-like OT candidates found in the photographic emulsion of archival plates were: (i) the result of an optical flash; (ii) not from any known atmospheric or celestial event; and (iii) a counterpart to a GRB at a previously known location (see for example: J. Greiner et al. (1987); A. N. Zytkow (1990); B. E. Schaefer (1990); J. Greiner (1992); B. E. Schaefer (1994); J. Greiner & E. Moskalenko (1994); R. Hudec (1993); F. J. Vrba et al. (1995); G. J. Fishman & C. A. Meegan (1995)).

Researchers understood that a valid candidate for a GRB optical counterpart from an archival plate must first be established to be the result of an optical flash and not (i) a plate fault: crack, dent, scratch, static discharge halo, glass corrosion, emulsion backing fragment, random cluster of grains (B. E. Schaefer 1990), endemic emulsion defect that creates a star-like false image (R. Hudec 1993; M. Varady & R. Hudec 1992; B. E. Schaefer 1990; J. Greiner et al. 1990, 1987), or aging blemish (J. Greiner et al. 1990); or (ii) an instrument or processing artifact: double exposure, pointing instability, or instrument vibration (R. Hudec 1993). Second, they needed to establish that the candidate was not due to any known real object: star (B. E. Schaefer 1990), nova or dwarf nova (R. Hudec et al. 1994), head-on meteor, satellite flash, aircraft flash (R. Hudec 1993; M. Varady & R. Hudec 1992), stellar flare, planetoid/minor planet, atmospheric event (R. Hudec 1993), or insect (e.g., firefly) (B. E. Schaefer et al. 1987).

Initial assessments about the validity of each star-like OT candidate centered on techniques that helped distinguish between a star-like plate artifact and a true optical transient. Ideally, a blink test was performed (which finds differences between two or more simultaneous photographs containing the same candidate). Without this, it was necessary to conduct an analysis of the physical plate itself using microscopy (500x) and microdensitometry (to obtain photodensity image profiles) with transmitted and reflected light (to look at grain structure in the emulsion), as well as CCD scanning techniques. These techniques were used in an effort to find: (i) a valid star-like 3-D structure in developed silver grains within the plate emulsion, and evidence of short duration (evidence of an optical flash); (ii) coma distortion (evidence of optical path); (iii) halos from atmospheric fog (evidence of optical path) (R. Hudec et al. 1994); and (iv) lack of a trailing (caused by telescope tracking errors) might indicate a short duration optical flash, but could also be a plate defect (B. E. Schaefer 1990). In the absence of multiple simultaneous plates, OT candidates with the supplementary support provided by these techniques were more likely to be accepted by scientific peers (R. Hudec 1993). However, several groups applied

these techniques to the same plate and arrived at different conclusions (R. Hudec 1993; F. J. Vrba 1996). By 1995, several OT candidates were still being championed as real optical flashes, although not unequivocally associated with GRBs (F. J. Vrba 1996).

Although nearly all plate defects could be rejected upon close inspection, a select few star-like candidates could not. Twenty years of dedicated searching for optical flashes near GRBs on physical, archival plates yielded five significant OT candidate sets (representing ten OTs). Among these, however, none could be “either definitely proved or definitely excluded” (R. Hudec 1993, pg 367) as real optical transients representing a new astronomical phenomenon, and none could be convincingly shown to be a GRB counterpart (F. J. Vrba 1996). The researchers were unable to rule out all of the alternate hypotheses, and thus could not disprove the null hypothesis in their search for the first example of a GRB optical counterpart.

In 1996, a dedicated satellite was launched to rapidly and accurately locate GRBs (B. J. McNamara & T. E. Harrison 1998), enabling potential OT counterparts to be imaged with CCD cameras in real-time and alleviating the need for the GRB community to work from the archival plates.

Digitization of the DSS POSS1 plates began in 1992 and they became available on CD-ROM in 1995; the SuperCosmos digitization of POSS1 became available in 2000. The physical plate set of SuperCosmos copy negatives is available for examination at the Royal Observatory, Edinburgh (N. Hambly & A. Blair 2024); many surveys have slightly inferior originals available to examine (D. Morgan 1995).

The DSS and SuperCosmos digital scans used in E. Solano et al. (2022) and B. Villarroel et al. (2025c) added additional pathways for processing-related artifacts to enter the picture, such as images of dust particles and emulsion backing fragments.

In light of the challenging results from two decades of GRB OT studies, and the very few optical transient candidates found, it is not clear how a search for alignments and correlations of optical flashes from non-anthropogenic technosignatures proceeds without first independently verifying that the detections in the dataset(s) represent optical flashes.

Expressing similar concerns, N. Hambly & A. Blair (2024) examined the intensity profile statistics (position, brightness, and morphology) of all objects on the POSS1-E plate E0070 containing the nine transients allegedly identified by B. Villarroel et al. (2021). They found a class of objects they designated as “spurious,” that are statistically distinctive, and morphologically

distinguishable from stars and other astronomical objects; e.g., they exhibit a smaller full-width at half maximum (FWHM) on average. They then trained a machine learning model to distinguish between stars, galaxies, and likely spurious (not within 5'' of a Gaia or Pan-STARRS DR1 catalog object) and applied it to plate E0070, finding $\sim 45,000$ stars, $\sim 27,000$ galaxies, and ~ 8000 spurious objects (including the nine “transients” from B. Villarroel et al. (2025c)). Their so-called spurious objects nominally belong to the same class as the so-called transient dataset ($N=298,165$) defined by E. Solano et al. (2022) and used in B. Villarroel et al. (2025c). B. Villarroel et al. (2025a) have since acknowledged that many of the unidentified SPF exhibit a smaller FWHM when compared with stars, but have countered that this is not unexpected for short-lived flashes from objects in high-altitude orbits, during a long-duration (50 min) exposure. The following questions remain unanswered after N. Hambly & A. Blair (2024): (i) whether optical flashes exhibit smaller FWHM on POSS1 plates; (ii) whether any of the 8,000 features selected on plate E0070 by N. Hambly & A. Blair (2024) represent an optical flash; and (iii) whether some categories of plate artifacts exhibit a smaller FWHM when compared to stars, on average.

3. DATA SOURCES

In this section, we describe (i) the publicly available datasets used for the analyses in this paper; and (ii) the publicly known properties of the related and as-yet unpublished datasets used by S. Bruehl & B. Villarroel (2025) and B. Villarroel et al. (2025c). Access to the unpublished datasets is not necessary for our evaluation of the analyses and claims in the papers under scrutiny. The relationships between these published and unpublished datasets are illustrated in Figure 1 and defined in Table 1, where “SVR22” stands for Solano, Villarroel, and Rodrigo (2022), “VEA25” stands for B. Villarroel et al. (2025c), and “BV25” stands for S. Bruehl & B. Villarroel (2025). We use our own naming convention when referring to datasets (see the symbol (“Sym.”) column in Table 1), which are not used in the papers we have cited.

3.1. Definitions

The POSS1-E plates comprise 937 individual exposures using the red-sensitive Kodak 103a-E plate emulsion, whose sensitivity peaks at 640 nm with a limiting magnitude of 20 (R. L. Minkowski & G. O. Abell 1963). This optical survey ran from November 11, 1949 to December 10, 1958 and covered the whole sky north of declination -33° . This survey captured exposures for

292 plates with footprints residing fully in the southern celestial hemisphere; 584 plates with footprints residing fully in the northern celestial hemisphere; and 61 with footprints that overlap the celestial equator. The DSS and SuperCOSMOS scans were made from two independent sets of glass copy negative plates made from a single set of glass copy positive plates, in turn made from the original glass negatives (N. Hambly & A. Blair 2024).

E. Solano et al. (2022) began with the DSS scans of the POSS1 survey and extracted an unpublished dataset A (see Figure 1) whose size was not reported, containing all SPFs that passed their initial automated detection pipeline including signal-to-noise thresholds, spike removal, high proper motion, and morphological symmetry constraints (see E. Solano et al. (2022)).

To efficiently remove known stars while accounting for proper motion between surveys, SPFs in A within $5''$ of catalog objects from Gaia DR3 (A. Vallenari et al. 2023) and Pan-STARRS DR2 (K. C. Chambers et al. 2019) were removed from A (along with an unknown number of proximate SPFs that were not stars) to obtain the subset S ($N = 298,165$). With the exception of one plate, plates whose footprints reside entirely within the southern celestial hemisphere were never sampled, or else SPFs from those plates were removed at this stage.

Dataset W ($N=171,753$) is the publicly available subset of S containing features located within $5''$ of NeoWISE infrared catalog objects (A. Mainzer et al. 2011) that appear to have no optical counterpart i.e., no catalog objects at the same location in the visible band. W therefore comprises an undetermined number of NeoWISE objects along with an undetermined number of incidentally object-proximate SPFs. We determined that no SPFs in W derive from plates whose footprints reside entirely within the southern celestial hemisphere. E. Solano et al. (2022) then filtered the set S by removing the set W , creating the set P (i.e., $P \equiv S - W$).

In a series of stages, E. Solano et al. (2022) removed SPFs from P to produce the published dataset we that have called set R for “remainder”. First, E. Solano et al. (2022) removed all SPFs residing within $5''$ of stars in additional optical and additional infrared astronomical catalogs (as described in E. Solano et al. (2022)). Then, likely asteroids and variable objects were removed. The remaining 9,171 SPFs were searched for digitization-related artifacts (such as imaged dust or loose emulsion particles) by comparing separate scans of separate glass copy negatives (DSS and SuperCosmos) of the same field; an additional 3,592 SPFs ($\sim 40\%$) were identified and removed in this way. We expect that this step also removed endemic faults and aging-related SPFs (such as plate corrosion) found on the DSS copy negative but not

found on the SuperCosmos copy negative. On the other hand, this would not have removed plate defects whose source was the original glass plate or the copy positive glass plate. Next, SPFs identified as high proper motion stars and as obvious artifacts (by manual inspection) were also removed. The resulting set R ($N = 5,399$) contains the unidentified SPFs least likely to be celestial objects, non-star-like plate artifacts, or digitization artifacts, and comprises less than 2% of the SPFs in S .

For unknown reasons, B. Villarroel et al. (2025c) and S. Bruehl & B. Villarroel (2025) did not use R . Instead, B. Villarroel et al. (2025c) provided ambiguous definitions of the four datasets used in its analyses (S , V , V' , and V''), which are generally not concordant with definitions in E. Solano et al. (2022). Set S is tied to its definition in E. Solano et al. (2022) by the reported size ($N = 298,165$).

B. Villarroel et al. (2025c) defined set V ($N = 107,875$) as $S - W$ with SPFs in the southern celestial hemisphere removed; this appears to be the same definition as our $P \equiv S - W$ because W contains no SPFs from plates whose footprints completely reside within the southern celestial hemisphere. This cannot be correct, however, since the count of SPFs in V is short by 18,537 in light of the sizes reported for S and W in E. Solano et al. (2022). We can only assume that V was sampled in some unknown way from P . Next, it can be inferred that removing the SPFs in the southern celestial hemisphere (on the equatorial plates) from set V yields set V' ($N=106,339$). Set V'' ($N = 22,314$) is defined as V' with SPFs near the plate edges removed. Detailed motivations for these inferences are supplied in Sections 3.2 and Appendix A.

Although S. Bruehl & B. Villarroel (2025) cited E. Solano et al. (2022) as the source of its primary dataset, R was not used in this case, either. This was instead the set V from B. Villarroel et al. (2025c), based on the reported size ($N = 107,875$).

Our study makes use of the following SPF datasets, all of which are publicly available: (i) set W ($N = 171,753$), consisting of SPFs near NeoWISE object locations; (ii) set R , the most highly vetted subset from E. Solano et al. (2022); and (iii) set M , which contains the nearly 90 million SPFs recorded in the POSS1-E and POSS1-O plates by the MAPS project (R. L. Pennington et al. 1993; J. E. Cabanela et al. 2003). MAPS discarded all features that did not appear in both the E (red band) and O (blue band) plates, in order to avoid recording scratches and other plate artifacts; the Galactic plane was also occluded ($|b| > 20^\circ$) to avoid features that blend together in crowded fields. We chose the MAPS project digitization for comparison because it

was independent of the DSS and SuperCOSMOS digitizations and because it records only very confident detections of celestial objects. We have also used the POSS1-E meta data ([STScI 2026](#)), as well as POSS1-E images in DSS and SuperCosmos scans (shown in Figures 2 and 9) and Pan-STARRS images (shown in Figure 2). Finally, we use the three sources cited in Bruehl and Villarroel (2025) for nuclear test dates ([NNSS 2023](#); [Wikipedia 2025](#); [CHERCA 2025](#)).

Figure 1 illustrates the relationship between the A , S , W , P , V , and R datasets defined in Table 1, which are defined or implied in [E. Solano et al. \(2022\)](#), [B. Villarroel et al. \(2025c\)](#), and [S. Bruehl & B. Villarroel \(2025\)](#). This also illustrates the ambiguity (dashed line and “?”) concerning the amount of overlap between the publicly available set R , which is the most vetted [E. Solano et al. \(2022\)](#) dataset, and V , which has not been released as of the time of this writing. We stress that the relationship between R and V has not been disclosed, and that access to V is not necessary for our evaluation of the analysis and claims in [B. Villarroel et al. \(2025c\)](#) and [S. Bruehl & B. Villarroel \(2025\)](#).

3.2. Principal uses and additional properties

Set S: [E. Solano et al. \(2022\)](#) removed 288,770 SPFs from the dataset S in the process of creating R because these resided within 5" of infrared and optical sources in multiple catalogs ([E. Solano et al. 2022](#)). For unstated reasons, [B. Villarroel et al. \(2025c\)](#) reverted to using the dataset S to search for clusters of aligned objects, reporting these in Table 3 of that study. We investigate these clusters in Section 4.5.

Set R: This set is the tiny residuum that survived the [E. Solano et al. \(2022\)](#) filter pipeline, which was designed to remove all known celestial objects and digitization-related artifacts from S . As the most highly filtered subset of A , we subjected R to closer scrutiny by manually examining cropped POSS1-E images and Pan-STARRS images of the same field (published online by the authors⁷; in what follows, we supply ID numbers for the filenames of downloadable images on this site). We reviewed 10% of the SPFs in R (i.e., 540 images), finding 12 that appear to be of objects with exceptionally high proper motion (i.e., exceeding the 5" search radius) that appear in the Pan-STARRS frame (1043, 1051, 1059, 1130, 1243, 1271, 1277, 1345, 1374, 1376, 1409, 1513), and 11 that appear to form part of an obvious artifact (1092, 1248, 1255, 1460, 1179, 1223, 1259, 1301, 1396, 1473, 1507). Examples of these are shown in Figure 2. We therefore estimate that between 4% and 5% (i.e.,

~ 25/540) of the objects in R are catalog stars or obvious artifacts, which suggests that the overwhelming majority are roughly symmetrical SPFs without a catalog match.

Set W: This published dataset comprises SPFs located within 5" of infrared NeoWISE catalog objects that are not visible in the optical catalogs, and which are not expected to be visible in POSS1-E except in rare cases where these objects are flaring red dwarfs ([E. Solano et al. 2022](#)). Therefore, W is the result of using a spatially uniform-random distribution of positions (a starfield) to sample the set S , and is the focus of our analyses in Section 4.

Sets W and R: We have used W and R to reevaluate the purported correlations related to the Earth's shadow and nuclear tests (see Sections 5 and 6, respectively). Both of these public datasets were sampled overwhelmingly from plates whose footprints completely reside within or overlap the northern celestial hemisphere ($N = 645$). We found a single plate (plate ID 0DA7, label E1526) containing SPFs in set R whose footprint resides entirely within the southern hemisphere. We infer that [B. Villarroel et al. \(2025c\)](#) removed SPFs in the southern celestial hemisphere ($N = 1,536$ or 1.4%) from V ($N = 107,875$) to arrive at V' ($N = 106,339$). The fraction of SPFs residing below the celestial equator in R is also 1.4%, and in W is 0.07%. This is important because: (i) this supports our inference about the size of the ambiguously-defined set V in relation to set V' (with southern-hemisphere SPFs removed) reported by [B. Villarroel et al. \(2025c\)](#); (ii) with the exception of one plate, it can be inferred that [E. Solano et al. \(2022\)](#) did not sample from plates whose footprints reside entirely within the southern celestial hemisphere when constructing set A , since there is no mention of removing southern hemisphere SPFs in that paper; (iii) we are able to infer the true number of observation days within the study window when evaluating the reported correlation between SPF occurrence and nuclear tests (see Section 6), which differs from that used by [S. Bruehl & B. Villarroel \(2025\)](#).

Set V: Given that set R is currently the most vetted dataset of unidentified SPFs, it is not clear why [B. Villarroel et al. \(2025c\)](#) and [S. Bruehl & B. Villarroel \(2025\)](#) resampled P ($N = 126,412$) to create a new set V ($N = 107,185$). Set P includes 116,607 SPFs within 5" of an optical catalog object and 410 SPFs within 5" of an infrared catalog object, which means V is known to comprise at least 91% SPFs that have not yet been distinguished from catalog objects. Furthermore, V has not passed through the [E. Solano et al. \(2022\)](#) scan artifact removal step. We estimate up to ~ 40% of the ob-

⁷ See <http://svocats.cab.inta-csic.es/vanish-possi/>

jects in V would be classified by [E. Solano et al. \(2022\)](#) as scan artifacts, based on the fraction identified and removed to obtain R as reported in that study (see Table 1).

We have also attempted to estimate an upper bound for the number of endemic plate emulsion defects in V based on previous experimental estimates of their rate of production. These experiments were conducted using plate emulsions distinct from those used in the POSS1 survey and the defects were manually identified (versus automatically identified using an image processing pipeline). These earlier studies showed that certain ubiquitous plate emulsion defects appear star-like ([M. Varady & R. Hudec 1992](#); [J. Greiner et al. 1987](#)). For example, [J. Greiner et al. \(1987\)](#) examined six laboratory plates that were first exposed to diffuse light without a starfield to simulate the sky background illumination, and which were then developed. Through visual inspection, they found endemic faults that could be mistaken for stars at an average rate of 0.066 per cm^2 . Furthermore, the number of emulsion defects per unit area was found to increase towards the edges of the plate. Using a similar procedure on plates with a different emulsion, [M. Varady & R. Hudec \(1992\)](#) found a rate of 0.377 per cm^2 . These rates would translate to 83 and 475 star-like faults per POSS1 plate ($35.5 \text{ cm} \times 35.5 \text{ cm}$), respectively. Since two sets of plate emulsions preceded the copy negatives that were compared to remove defects, we double these rates to estimate of the number of these artifacts that could reside in both the DSS and SuperCosmos scans. Since V is derived from set A sampled from approximately 645 plates, we estimate that A could have contained a population of roughly 107,000 to 612,000 star-like emulsion faults. The initial morphological filter in [E. Solano et al. \(2022\)](#) would not have removed these symmetrical features, and some unknown fraction would have been removed incidentally because of proximity to Gaia, PS, or NeoWISE catalog objects. If the Kodak 103a-E plate emulsion behaves in a similar way to the emulsions evaluated in these experiments, then it is plausible that endemic plate emulsion defects comprise a significant fraction of the SPFs in V ($N = 107,875$).

[B. Villarroel et al. \(2025c\)](#) used V to search for correlations of SPFs with terrestrial shadowing. [S. Bruehl & B. Villarroel \(2025\)](#) also used V to look for correlations between the days on which SPFs were recorded on POSS1-E plates and days with nuclear tests and UAP reports. More discussion concerning the ambiguous definition of V can be found in Section 7 and Appendix A.

Set M: We have compared the spatial distribution of likely celestial objects in M (i.e., residing in both POSS1-E and POSS1-O plates) with the spatial distribution of SPFs in R and W in Section 4. We have done this in order to examine patterns noted in R and W that are not apparent in M ; i.e., that cannot be attributed to variations in the sensitivity of the optical system, the distribution of known celestial objects, or the astronomical viewing conditions on any given POSS1 observation day.

POSS1-E plates: There is no mention in [E. Solano et al. \(2022\)](#) about the removal of SPFs or plates imaged in the southern celestial hemisphere, which leaves unexplained why the southern hemisphere plates were not sampled or, if they were sampled, why these SPFs were removed and at what stage in the construction of sets S, P, W, R and V .

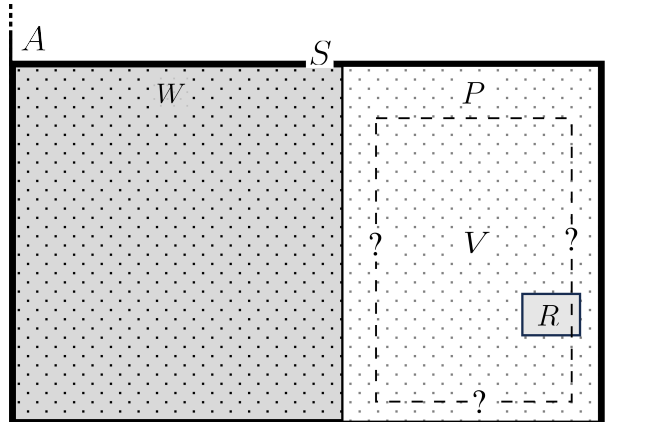


Figure 1. Diagram illustrating the relative sizes and overlap relationships of the SPF datasets defined in Table 1. The dashed line and “?” here represent our uncertainty about the degree of overlap between V (the main focus of calculations in [B. Villarroel et al. \(2025c\)](#) and [S. Bruehl & B. Villarroel \(2025\)](#)) and R (the vetted “remainder” of unidentified objects, defined in [E. Solano et al. \(2022\)](#)). The shaded subsets R and W are publicly available.

4. SPATIAL DISTRIBUTION

In this section, we consider five aspects of the spatial distribution of the SPFs in R and W that provide information about their origin: (i) the variation in SPF counts per plate; (ii) their distribution with respect to the boundaries of photographic plates as a function of displacement from the plate centers; (iii) the nonrandom spatial distributions of SPFs on some plates, in which SPFs tend to avoid well-defined zones or reside mainly within simple geometrical shapes; and (iv) the SPF distribution across the sky. Finally, we also address (v) the

Sym.	Summary	Size	Definition	Notes
A	All SPF	?	All SPF extracted from POSS1-E plates	Defined in SVR22. “ A ” is for “all.”
a_0		?	SPFs within $5''$ of objects in Pan-STARRS DR2 and Gaia EDR3 optical catalogs	These SPFs were identified for removal because they may represent catalog stars with up to $5''$ of proper motion. An unknown number of proximate plate artifacts were likely incidentally matched.
S	PS & Gaia removed	298,165	$A - a_0$	Defined in SVR22. Used to search for clusters of SPFs with statistically significant alignments in VEA25. “ S ” is for “ Solano et al. (2022) .”
W	Matched to NeoWISE objects	171,753	SPFs in S within $5''$ of NeoWISE objects, without an optical counterpart.	Defined in SVR22. Identified as possible flaring dwarf stars (SVR22). Used in our study to understand the sampling and spatial distribution of SPFs. “ W ” is for “ WISE ” in NeoWISE. Published online. [†]
P	PS, Gaia, NeoWISE removed	126,412	$S - W$	The result of removing from A the SPFs matched to objects in the “primary” catalogs (Pan-STARRS, Gaia, NeoWISE). “ P ” is for “ primary catalogs removed ”.
p_0		116,607	SPFs matched to other optical catalogs ($< 5''$)	See Solano et al., (2022) for details.
p_1		410	SPFs matched to other infrared catalogs ($< 5''$)	See Solano et al., (2022) for details.
p_2		224	189 asteroids and 35 variable objects in $P - (p_0 \cup p_1)$	
p_3		3,592	SPFs in $P - (p_0 \cup p_1 \cup p_2)$ that appear in DSS but not SuperCosmos scans	SPFs that appeared in one set of scans but not the other were interpreted as artifacts introduced by the scanning process (e.g., dust), or as endemic plate flaws in DSS scans of the glass copy negatives.
p_4		180	178 high proper motion stars and 2 artifacts in $P - (p_0 \cup p_1 \cup p_2 \cup p_3)$	The two artifacts were recognized via visual inspection.
R	Remainder unidentified SPF	5,399	$P - (p_0 \cup p_1 \cup p_2 \cup p_3 \cup p_4)$	Defined in SVR22. This is the most vetted dataset of unidentified SPFs. Used in our study to find expected vs. actual frequency of SPFs in the terrestrial shadow, and estimate the correlation with timing of nuclear tests. “ R ” is for “ remainder .” Published online. [‡]
V	PS, Gaia, NeoWISE removed	107,875	$P - ?$ where “?” is a subset of P that is nowhere defined.	Ambiguously defined in VEA25. Defined as identical to P , with expected size 126,412. Used in VEA25 to calculate relative frequency of SPFs in Earth’s shadow and in BV25 to estimate correlation with nuclear tests. “ V ” is for Villarroel et al. (2025)
v_0		1,536	SPFs in V with dec. $< 0^\circ$	1.4% of SPFs in V that reside in the southern celestial hemisphere
v_1		85,561	SPFs in V located $> 2^\circ$ away from plate centers	This set was intended to encompass clusters near plate edges.
V'	PS,G,NW, dec. $< 0^\circ$ removed	106,339	$V - v_0$	Southern hemisphere SPFs removed from V . Used by VEA25 to estimate relative frequency of SPFs in Earth’s shadow.
V''	Plate edges also removed	22,314	$V - (v_0 \cup v_1)$	SPF at edges of plates removed from V' . Used in VEA25 to estimate the background number density of SPFs and relative frequency of SPFs in Earth’s shadow.
M	MAPS catalog	89.1M	SPFs with $ b > 20^\circ$ in E and O plates	Defined in Pennington et al. (1993); SPFs from the MAPS POSS1-E scans with absolute galactic latitude $> 20^\circ$. Published online.*

Table 1. Datasets analyzed or discussed in the text. These include datasets of Selected POSS1-E Features (SPFs) defined in [E. Solano et al. \(2022\)](#) (SVR22) and [B. Villarroel et al. \(2025c\)](#) (VEA25) and also used in [S. Bruehl & B. Villarroel \(2025\)](#) (BV25). Also defined is the M dataset of likely celestial objects measured from the POSS1-E and POSS1-O plates described in [R. L. Pennington et al. \(1993\)](#) and [J. E. Cabanela et al. \(2003\)](#). Note that we have used these abbreviations: PS \equiv Pan-STARRS, G \equiv Gaia, and NW \equiv NeoWISE.

[†]Retrieved on 2025-12-08 from <http://svocats.cab.inta-csic.es/vanish-neowise/>

[‡]Retrieved on 2025-12-08 from <http://svocats.cab.inta-csic.es/vanish-possi/>

*Retrieved on 2025-12-08 from <https://aps.umn.edu/catalog/download/>

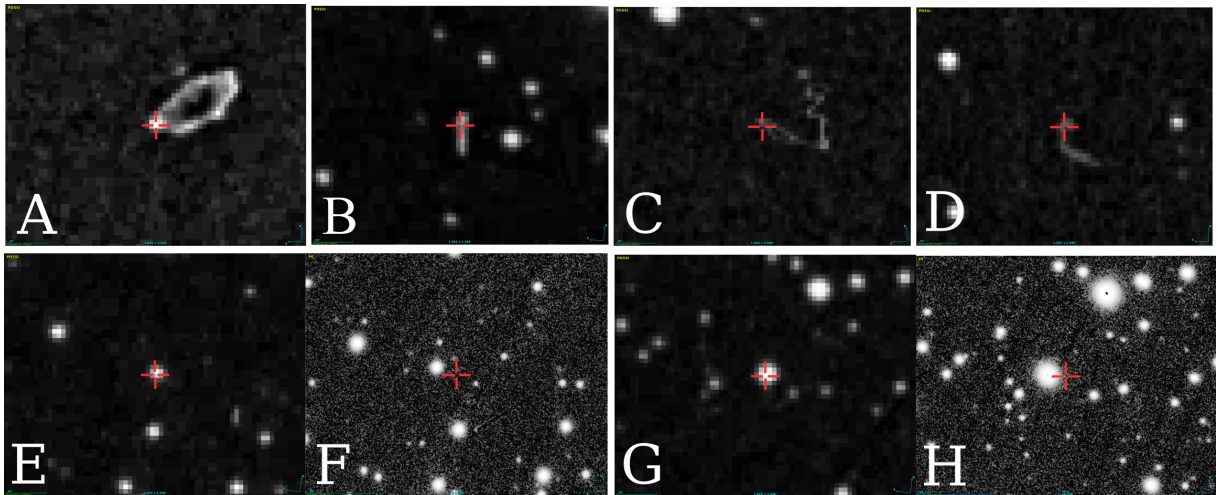


Figure 2. Examples of Selected POSS1-E Features (SPFs) in R ($N = 5,399$), the most vetted subset of S ($N = 298,165$) published by E. Solano et al. (2022). The red crosses at the center are $\sim 10''$ in diameter. We have identified these features as follows: (i) clear artifacts or defects that do not resemble objects visible in a Pan-STARRS image of the same field (A (object 1092), B (object 1179), C (object 1223), D (object 1248)); and (ii) clear examples of an object that was incorrectly identified as having vanished (object 1043 in E vs. F, and object 1051 in G vs. H, where E and G are POSS1-E images and F and H are Pan-STARRS images), probably on account of displacement from high proper motion. Based on 540 objects examined, cases of this sort comprise 4–5% of R ($N = 5,399$). The images are available online from <http://svocats.cab.inta-csic.es/vanish-possi/>.

sporadic alignments of SPF s reported in Table 3 of [B. Villarroel et al. \(2025c\)](#).

Before proceeding, we define the phrase “spatially uniform-random distribution” or simply “uniform-random” as referring to the spatial distribution resulting from a Poisson point process: e.g., the spatial distribution characteristic of star fields. We define “nonrandom” as any spatial distribution of features that, in principle, can be distinguished from “uniform-random” using a statistical test.

4.1. Variation in counts per plate

We examine the variation of counts per plate as part of assessing assumptions implicit in the analyses of [B. Villarroel et al. \(2025c\)](#) and [S. Bruehl & B. Villarroel \(2025\)](#) about what factors supposedly influence the distribution of SPF counts in time and space, such as the terrestrial shadow and nuclear tests. Primary sources of variation in counts per plate should be characterized, modeled, and subtracted *before* second-order effects are considered. In particular, we might expect the number of SPF s per plate to vary for two primary reasons. First, if the SPF s represent a population of stars not removed by prior filtering, then we expect (i) a roughly uniform-random distribution with an overall increase in number density with decreasing distance from the Galactic plane; and (ii) slight variations associated with variations in the astronomical viewing conditions (i.e., more stars are detected under favorable atmospheric conditions with less turbulence blur). Alternatively, if the SPF s represent plate artifacts, the distribution will depend on the processes that tend to create these features, and upon how the impact of these processes varies from plate to plate. This may in turn depend on how the plates were manufactured, exposed, developed, stored, and handled, and how often they have been accessed. Finally, we should consider that the digital scanning process may also introduce artifacts, such as by introducing images of dust or debris in the scanner or on the plate surface. [E. Solano et al. \(2022\)](#) removed digitization artifacts only after removing over 117,000 SPF s from set P ($N=126,412$) when constructing set R ($N = 5,399$), whereas the removal of digitization artifacts was neither explicitly described nor mentioned in [B. Villarroel et al. \(2025c\)](#) or [S. Bruehl & B. Villarroel \(2025\)](#) as part of the sampling of V ($N = 107,875$) from P .

Since the published tables for R and W do not list the plate of origin for each SPF, we have determined this as follows: for each SPF, we find all plate centers within 3° in declination, and then select the plate whose center is nearest in horizontal separation. We have noted all SPF s whose position is overlapped by the fields of view

of multiple plates, and which cannot be unambiguously assigned to a single plate, so that we can remove these in the analyses discussed in later sections.

We found that counts of SPF s per plate in both W and R exhibit enormous variation. In W , the number of SPF s per plate ranges from zero to 2,149 (Plate 090R), with an average of 257.5 and standard deviation of 337.2. In R , the number of SPF s per plate ranges from zero to 105 (Plate 08BW), with an average of 8.1 and standard deviation of 10.3. Figure 3 shows the cumulative fraction of SPF counts as a function of the total fraction of plates, ranked in order of decreasing counts from left to right. The first datum plots as ~ 0.012 on the y axis because the first plate, being the most crowded, comprises over 1% of all the SPF s in the dataset. This figure illustrates that 50% of the plates contain nearly 90% of the SPF s in W .

We display the same plot for the M dataset in Figure 3, which shows a more gradual increase across the sample, but which still represents a significant departure from a uniform-random distribution (dotted line), possibly on account of variations in astronomical viewing conditions. Recall that all of the SPF s in M correspond to likely celestial objects, as these are apparent in both the E and O plates (red and blue bands). Another potential reason for the difference in distributions is that whereas M omits the bright zone within 20° of the Galactic plane, S and its subsets (e.g., R and W) were sampled from throughout this region. That is, it is possible that the variation in SPF counts per plate in S has been more strongly affected by the increased number density near the Galactic plane. This could happen if (i) the SPF count comprises previously uncatalogued stars (e.g., flaring red dwarf stars), or (ii) the high number density of stars in this region result in blended objects with inaccurate centroid positions that frustrate the identification and removal of catalog objects.

4.2. Distribution with respect to plate boundaries

We will focus in this section on spatial distribution of SPF s within plates in set W ($N = 171,753$) because (i) it is publicly accessible; (ii) it is large enough to clearly see patterns in relation to the plate center and boundaries; and (iii) it is a majority subset of the set S used by [B. Villarroel et al. \(2025c\)](#) to search for linear clusters. Moreover, (iv) it will have retained some characteristics of S , the parent dataset of V , which is the focus of the analyses in [B. Villarroel et al. \(2025c\)](#) and [S. Bruehl & B. Villarroel \(2025\)](#). This is because W is effectively a dense, uniform-random sampling of the set S ; i.e., it consists of SPF s residing within $5''$ of NeoWISE infrared catalog objects, which are not expected to be visible in

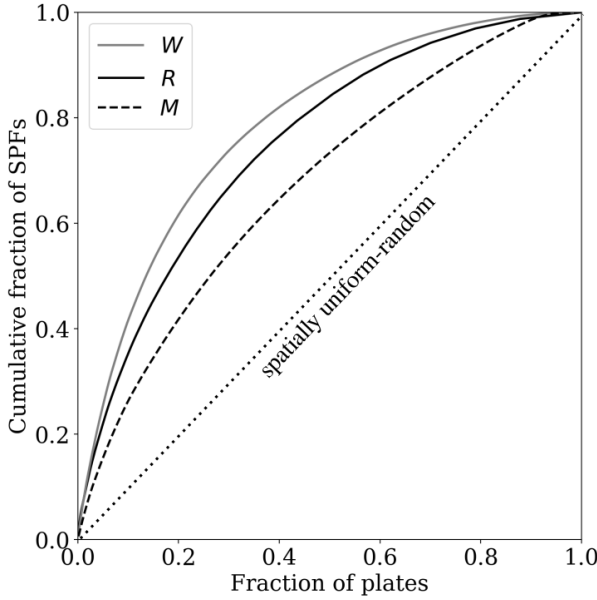


Figure 3. Cumulative distribution function of SPF counts as a function of the total fraction of plates, ranked in order of decreasing counts from left to right, for W , R , and M . In the case of W , roughly 20% of the most crowded plates contain over 60% of all SPFs. M is more uniform in terms of how SPFs are distributed across plates; this is partly because all SPFs in M are likely celestial objects, and because the Galactic plane was occluded when this dataset was sampled. The curve still represents a significant departure from a uniform-random distribution (dotted line), possibly associated with variations in astronomical viewing conditions. The discussions of spatial variability in Sections 4.2 and 4.3 suggest there may be multiple factors contributing to the spatial variation in SPF counts shown in R and W , arising from (i) how plates are manufactured, stored, scanned, and handled, or (ii) how datasets were constructed in [E. Solano et al. \(2022\)](#).

POSS1-E plates unless (in rare cases) they are flaring red dwarfs ([E. Solano et al. 2022](#)). In summary, we focus here on the published dataset W because of what we can learn about characteristics of the unpublished sets S and V .

In Figure 4, we have plotted the positions of SPFs in W on selected plate fields that exhibit distinctive patterns, which in some cases bear a clear relationship to the plate boundaries. We have marked the SPFs with ambiguous plate assignments in red. These plates contain a wide range of SPF counts, most of them significantly exceeding the average of W 's 270 SPFs per plate. All SPFs in W reside within 5" of NeoWISE infrared catalog star positions and were removed from S when constructing V for this reason ([E. Solano et al. 2022](#)). As Figure 4 shows, and as we demonstrate quantitatively

later in this section, the distribution of SPFs from W is not spatially uniform-random, which is the expected spatial distribution of a star field. This suggests that the underlying distribution of SPFs in the parent set S is also strongly nonrandom and also bears a clear relationship to the plate boundaries. Furthermore, the fact that the intra-plate distribution of SPFs in W is far from uniform-random suggests that the large search radius (5") and large number density of NeoWISE objects has resulted in sampling many noncelestial objects that were incidentally matched.

Figure 4 reveals that there is a strong spatial variation within individual plates that is distinct from the plate-to-plate variation in astronomical viewing conditions and proximity to the Galactic plane. Notably, on plates with large SPF counts, these appear to be sometimes concentrated in clusters. To characterize the spatial distribution of SPFs within plates in W , we have calculated the Clark-Evans ratio (ρ) for each plate ([P. J. Clark & F. C. Evans 1954](#)). This is defined as

$$\rho \equiv \frac{\bar{r}_{\text{obs}}}{\bar{r}_{\text{CSR}}}, \quad (1)$$

where \bar{r}_{obs} is the observed average nearest neighbor distance between SPFs in a given plate, and $\bar{r}_{\text{CSR}} \equiv 1/2\sqrt{\lambda}$ is the average nearest-neighbor distance for a special case of the uniform-random distribution (generated by a Poisson point process) with average number density λ ([P. J. Clark & F. C. Evans 1954](#)). The special case is that of complete spatial randomness (CSR), defined as the spatial distribution resulting from a homogeneous Poisson point process on an infinite domain. Because photographic plates have a finite extent, the nearest neighbor distance of SPFs near plate edges is larger than average, causing ρ to be slightly more than 1 for points that are spatially uniform-random. The case $\rho \gg 1$ implies a spatially underdispersed distribution (relatively regular spacing), while $\rho < 1$ implies overdispersion (clustering).

We have computed ρ on all of the plates containing SPFs for sets W and M . Set M was downsampled to 0.2% of its normal size to reduce computation time ($N \sim 170,000$), and so that its size is comparable to that of W ($N = 171,753$). Set R has been omitted from this analysis on account of its small size, with the result that ρ becomes a noisy statistic. The scatter plots of SPFs in set W for the plates in Figure 4 have been labeled with estimates of ρ , which ranges from 0.49 to 0.80 for these examples. Figure 5 contains a histogram of ρ for plates in M and W . As expected, the spatial distribution of SPFs in the spatially uniform-random set M , consisting of SPFs that are very likely celestial in origin because they occur in both the O and E plates, usually result in

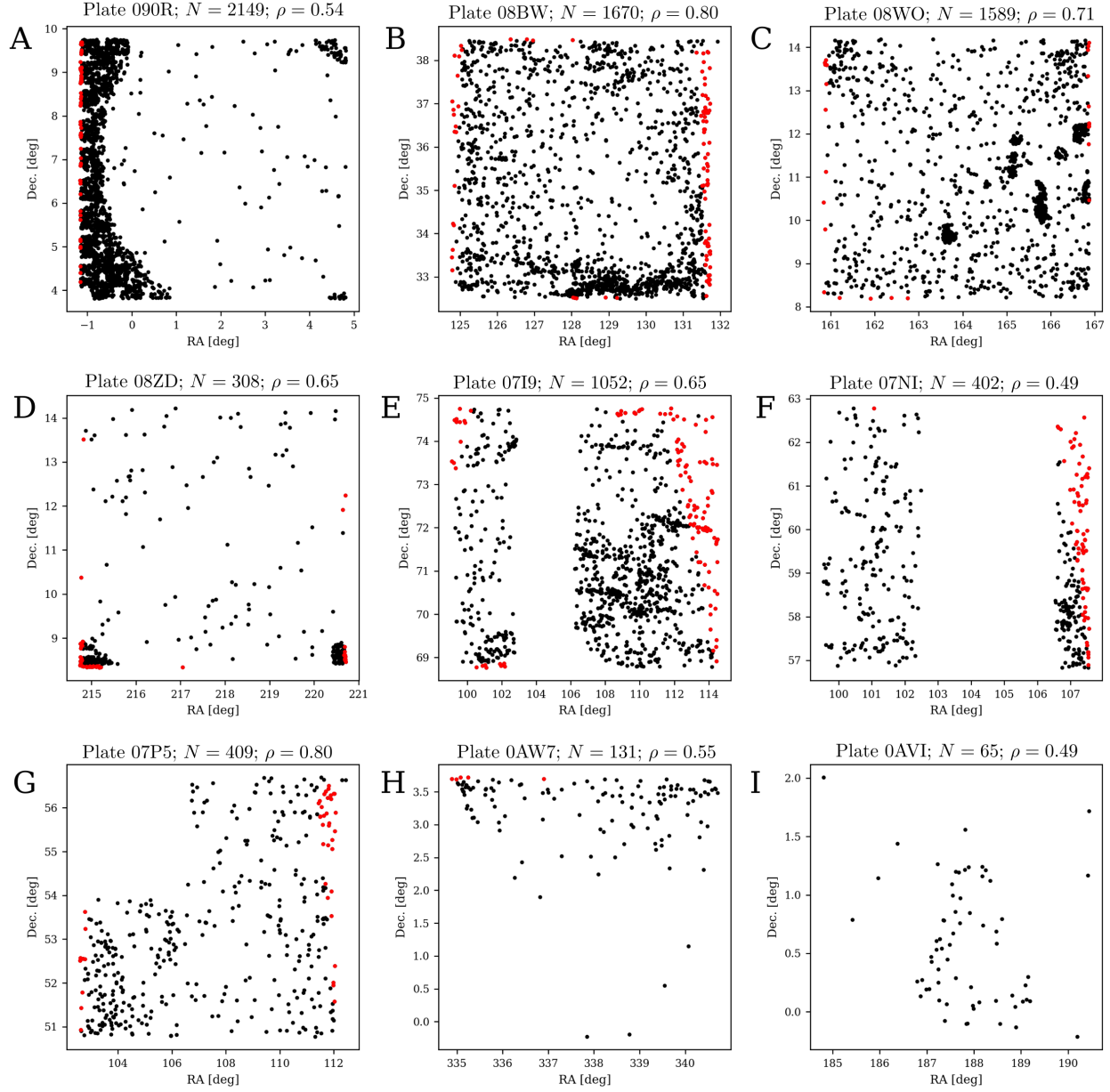


Figure 4. Scatter plots of SPFs from W on nine plates that exhibit distinctive patterns. Red dots signify SPFs that could not be unambiguously assigned to the plate in question because of overlap with the neighboring plate's field of view (and hence confined to the edges). These patterns are not visible in the dataset M of SPFs that appear in both E and O plates (i.e., likely celestial objects), suggesting that they are unrelated to nonuniform sensitivity of the instrumentation or photographic medium. The geometric patterns and relationship to plate boundaries strongly suggest (i) a physical process that has templated the spatial distribution of SPFs, such as a surface that has come into contact with the plate, or a region that has been preferentially exposed to processes that tend to degrade the medium over time; or (ii) a spatial filter applied when processing the data. We have plotted SPFs from W because (i) it is publicly accessible; (ii) it is large enough for these patterns to be visible, and (iii) because it is a dense, uniform-random sample and majority subset of S , the parent set of set V analyzed by [S. Bruehl & B. Villarroel \(2025\)](#) and [B. Villarroel et al. \(2025c\)](#). Each plate is labeled with the plate ID, the number of SPFs on the plate, and the value of the Evans-Clark ratio ρ , which is smallest for the most overdispersed (clustered) distributions.

values of ρ slightly above 1 (modal value 1.04). By contrast, ρ for plates in the set W are widely distributed, peaking at modal value 0.89. SPF s in W are mostly overdispersed and exhibit moderate to significant clustering. The scatter plots shown in Figure 4 are examples of significant overdispersion, sampled from the left-hand tail of the histogram in Figure 5 for set W .

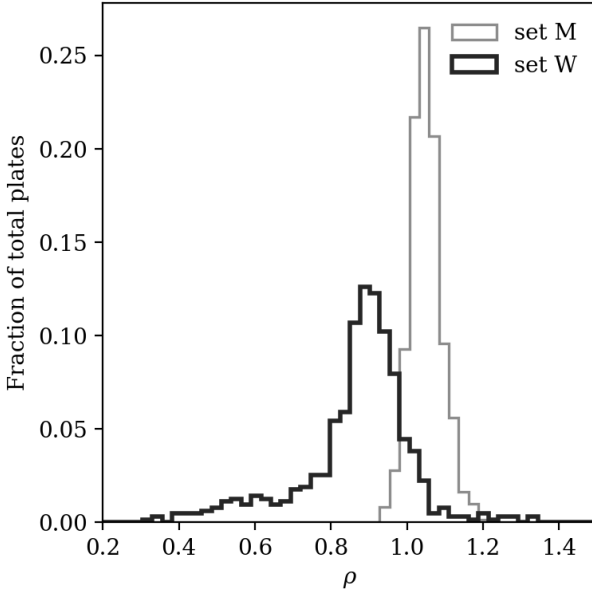


Figure 5. Histograms of the Evans-Clark ratio ρ calculated for each plate, for SPFs in sets M and W . As expected for a uniform-random distribution of points on a finite domain, ρ is typically slightly above 1 for set M , comprising SPFs of likely celestial origin because they appear in both the POSS1-E (red band) and POSS1-O plates (blue band). The distribution of SPFs in W is dominantly overdispersed (clustered), with $\rho < 1$ for most plates. See Figure 4 for scatter plots of SPFs on individual plates with significant overdispersion, labeled with the estimated ρ .

Next, we characterized the average spatial distribution within photographic plates. For the M , W , and R datasets, we computed the displacement in decimal degrees of SPFs with respect to the center of each plate in declination and right ascension. The latter was multiplied by the cosine of the declination to compute true east-west displacement on the sky. These displacements were used to compute a normalized radial density profile in Figure 6 for sets M , W , and R . For each data set, we have also broken down the spatial distribution of the total SPF counts across all plate fields into a median background plus a nonrandom excess. In Figure 7, we have subtracted the median background SPF count within 2-D bins in order to visualize the excess SPF

counts; this is shown in parts A, B, and C for sets M , W , and R , respectively. In plotting parts B and C, we have used only the SPFs that can be unambiguously assigned to plate footprints.

The distribution for set M is consistent with expectations for telescopic observations of star fields: the centers of photographic plates tend to contain slightly more counts than the perimeter owing to the effect of vignetting near the margins. By contrast, the excess in W and R shows the opposite pattern, with the number density of SPFs increasing with distance from the center of the plates, and is therefore highest at the corners and edges. The amplitude of this radial increase, as a fraction of total counts, is also much larger than the amplitude of the variation in M (Figure 6). Recall that R supposedly contains only features that are not identifiable as plate artifacts, digitization artifacts, or celestial objects, and so it is difficult to form an expectation in advance about the intra-plate spatial distribution. By definition, all SPFs in W are located in close proximity to the positions of NeoWISE objects. Nevertheless, W exhibits a pattern that is inconsistent with the expectation of a uniform-random distribution for a star field on an individual plate: i.e., it does not resemble the distribution of SPFs in M .

The observed pattern for R and W instead suggests a distinct generative process that depends on proximity to plate boundaries. As part of the GRB-related efforts to understand plate faults, J. Greiner et al. (1987) examined laboratory plates that had been exposed to diffuse light equivalent to sky background illumination, and which were then developed. Using different emulsions and plates, they found endemic faults at a rate that translates to 83 faults per area of a POSS1 plate ($35.5 \text{ cm} \times 35.5 \text{ cm}$) that were difficult to distinguish from ideal stars or slightly distorted stars. These faults included point-like objects indistinguishable from stars, oblong objects indistinguishable from stars with trails, and objects with comas located on the outer edges of plates that resembled a normal star with slight distortion. The number of faults increased towards the edge of the plate and also with decreasing brightness. Other mechanisms for generating non-random excesses of SPFs on the edges of plates have not been experimentally examined; these include the contamination or degradation of the emulsion through handling of plates by the corners and edges. The distributions of SPFs shown here are plausibly related to the manufacture, processing, degradation, or digitization of the plates and unrelated to luminous or illuminated objects in the telescope's field of view.

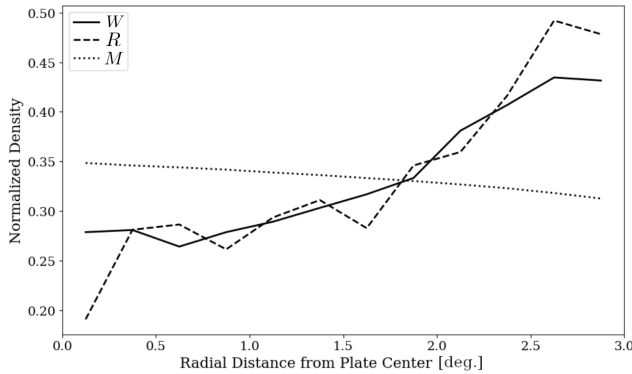


Figure 6. Radial density profiles for the W (solid), R (dashed), and M (dotted) datasets. Densities were calculated in circular bins of 0.25° with radii denoting the angular distance from plate centers. All distributions were normalized for easy visual comparison of their shapes. The W and R distributions show an increasing density of SPFs away from plate centers, in qualitative agreement with the experimental results of J. Greiner et al. (1987), who found that the number density of endemic plate emulsion defects increases with distance from plate centers. By contrast, M exhibits a slight and gradual decline with radius, indicating a mostly uniform number density combined with the effect of vignetting, as expected for a star field.

4.3. Templatizing and spatial filtering

In some cases, the distribution of SPFs within plates exhibits patterns and clusters that are qualitatively distinct from the mean pattern described in the previous section. A prominent example occurs very near the celestial meridian and equator in the plate with the largest number of SPFs (Plate 090R; $N = 2,149$; part A in Figure 4), where the majority of SPFs are located between the boundaries of the plate and an oval that is partially inscribed within it. The origin of these patterns is not known. Other plates exhibit rectangular voids (part G) or band-like vertical gaps (parts E and F). We also find examples of tight clusters within central regions of a plate (part C) or at the corners (part D). A few plates exhibit a density gradient with highest density at one edge, decreasing toward the opposite edge (part H).

That some plates exhibit patterns bearing a clear relationship to plate boundaries (e.g., clustering near edges) and/or the celestial coordinate system (e.g., voids and clusters exhibiting horizontal and vertical edges, parallel to lines of constant right ascension or declination), suggests the action of generative mechanism(s) that relate to the manufacture, processing, curating, or digitizing of the plates, rather than to lights in the sky.

We hypothesize that the distribution of SPFs in some regions of some plates are “templatized” by contact with objects or surfaces, or by preferential exposure to a pro-

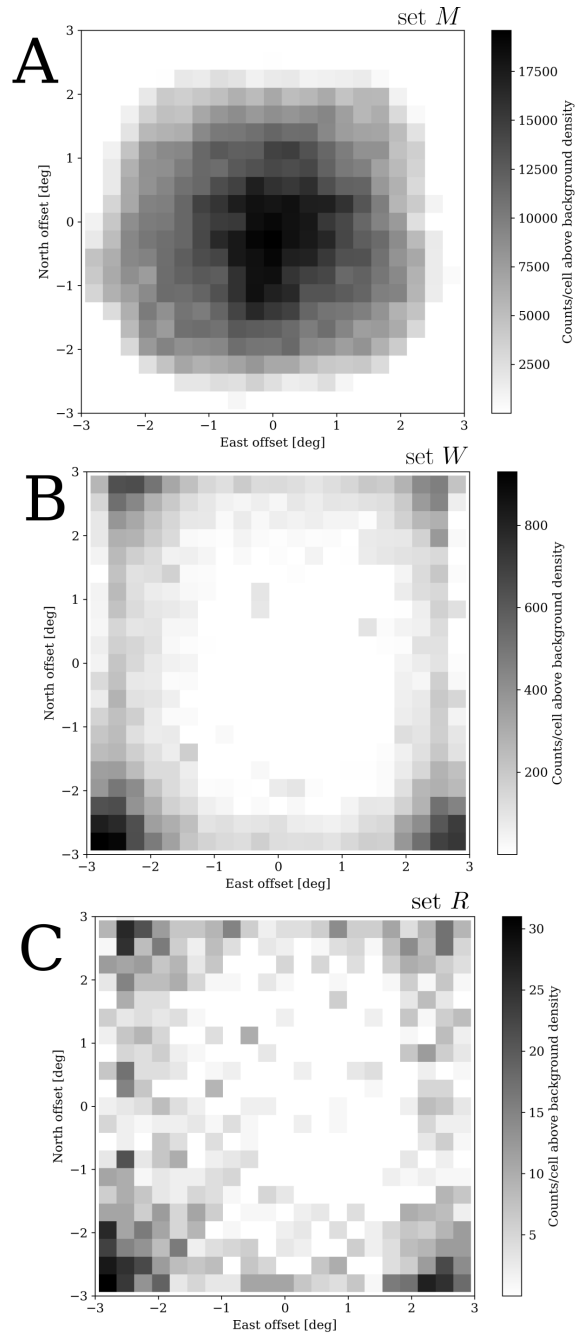


Figure 7. Histograms (2-D) of SPF counts in excess of the median background as a function of offset from plate centers for (A) set M (likely celestial objects that appear in both O and E plates; see J. E. Cabanela et al. (2003)); (B) set W , which reside within $5''$ of the positions of NeoWISE infrared catalog objects (E. Solano et al. 2022); and (C) set R , comprising unidentified SPFs. The set M distribution peaks in the center, possibly on account of the effects of vignetting at the margins. The distributions for set W and R peak in the edges and corners, and are qualitatively consistent with the expected pattern for endemic plate emulsion defects (J. Greiner et al. 1987).

cess that tends to degrade the photographic medium. The fact that SPF_s occur within regions with clear boundaries, or else avoid regions with clear boundaries, suggests that contact or exposure-based templating may play an important role in the production of SPF_s on many other plates, where the contact (or exposed) surface mostly or completely covered them. An example zone of avoidance is visible in the upper-left corner in part G of Figure 4. Based on inspection of multiple plates, the vertical stripes in parts E and F span the interval in right ascension from roughly 103° to 107° and cross plate boundaries; a second stripe from roughly 86° to 98° also crosses plate boundaries. Both of these features are further discussed in Section 4.4.

We emphasize the importance of answering the following questions. First, why do SPF_s in some cases appear to reside in clusters or regions of higher number density with clear boundaries, and why do they sometimes appear to avoid regions with clear boundaries? Second, why do these overdense regions and empty regions in some cases appear related to the plate footprint or the celestial coordinate system (e.g., Plate 090R in part A of Figure 4)? Third, what does this imply about the production of SPF_s in general? These questions should be answered as part of the essential data validation process.

4.4. Distribution across the sky

In this section, we examine significant variation in SPF number density on the scale of the entire sky. We have plotted the on-sky distribution of the number density of SPF_s from set *M* in part A of Figure 8 (i.e., likely celestial objects that appear in both O and E plates); we have plotted the number density of SPF_s from *W* in part B and from *R* in part C. As mentioned, J. E. Cabanella et al. (2003) occluded a buffer zone surrounding the Galactic plane to avoid blended objects in crowded fields when constructing *M* ($|b| > 20^\circ$). By contrast, E. Solano et al. (2022) does not specifically mention avoiding the Galactic plane while sampling.

We have shown the all-sky map of SPF number density in Figure 8 to call attention to the significant variation in this quantity across the sky in the E. Solano et al. (2022) data sets, and especially the vertical stripe between roughly RA = 90° and RA = 105° for both *R* and *W*. Closer inspection of the plate-framed scatter plots (as shown in Figure 4, parts E and F) suggests that this stripe consists of two bands, from roughly RA = 87° to RA = 98° and a second, narrower band from RA = 103° to RA = 107° . This stripe lies largely in the galactic occlusion zone of set *M*, but no such stripe is visible in scatter plots of SPF_s in *M* near the poles.

Therefore, this feature in *W* and *R* does not appear to have resulted from a failure of the instrument to faithfully record astronomical objects in this region.

We considered four possible explanations regarding the origin of the stripes: (i) *The SPF_s were incompletely sampled when the set A was assembled by E. Solano et al. (2022) in the first place, or when the DSS or SuperCOSMOS scans were acquired.* This appears unlikely because the stripes do not correspond to plate boundaries: they cross plate boundaries and only partially overlap some plates (see Figure 4, parts E and F). Note that plate boundaries become staggered as the sky area narrows near the poles, and yet the stripes span the full range of declinations: they are not offset or shifted at plate boundaries. Moreover, the striping did not affect set *M*, which was independently scanned; this suggests the stripes are not an intrinsic property of the plates themselves. (ii) *The stripes are the result of how the plates were stored, maintained, and handled.* This seems unlikely because it is hard to imagine how any of these activities could create a stripe that traces lines of roughly constant right ascension and which cross plate boundaries, especially given the staggered arrangement of plate footprints on the sky. (iii) *The POSS1 telescope observations overlapping the stripe were captured during periods of time when SPF_s, if they represent luminous or illuminated objects in the telescope's field of view, were less abundant in the sky.* This can be confidently ruled out because the plates overlapping the stripes were captured throughout the duration of the POSS1 survey (8 years). Also, as mentioned already, the stripes only partially overlap the plates, ruling out a time dependence. This leaves the least unlikely cause: (iv) *SPF_s within the stripes were filtered out during the processing steps that led from set A to sets W and R in E. Solano et al. (2022).* It is not clear why this interval would be singled out for suppression, intentionally or by accident.

We call attention to this feature of the on-sky distribution because analyses in B. Villarroel et al. (2025c) and S. Bruehl & B. Villarroel (2025) implicitly assume that *V* is completely and uniformly sampled (i.e., no part of the north celestial hemisphere was omitted when SPF_s were selected) and faithfully records the distribution of SPF_s across the sky. This assumption is essential for one of the key claims in B. Villarroel et al. (2025c), which reports a deficit of SPF_s from set *V'* in the Earth's shadow, as discussed in the next section. This is also significant for interpreting the background rate of SPF_s made in the same paper. An incomplete or nonuniform sampling would affect correlation statistics between SPF occurrence and any other phenomena, such as nuclear tests S. Bruehl & B. Villarroel (2025).

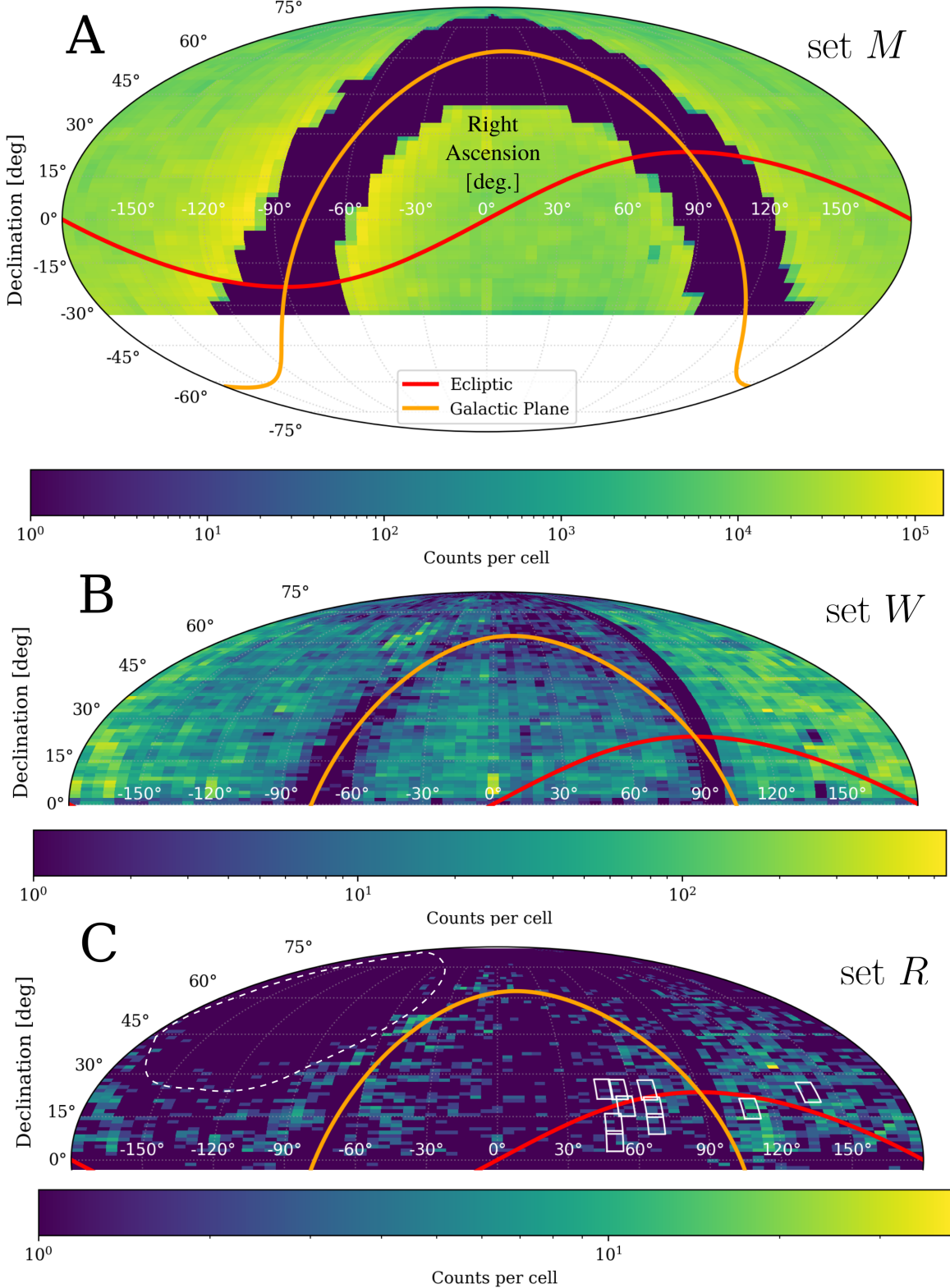


Figure 8. Plots of the number density of SPF counts on the celestial sphere in (A) set M , (B) set W , and (C) set R . The distribution of SPF counts in parts B and C reveal a vertical band with a deficit of SPF counts between 90° and 105° ; this remains apparent following aggressive filtering in R . The white boxes in (C) show the outlines of plates estimated to overlap Earth's shadow during the observation window, as discussed in Section 5. B. Villarroel et al. (2025c) reported a deficit of SPF counts from set V' within these plates. The red line shows the ecliptic, the orange line is the Galactic plane, and the dashed white line highlights a marked depletion north of the celestial equator in the western hemisphere when compared to the eastern hemisphere.

There are marked similarities and differences evident from comparing the spatial distributions of W and R (see parts B and C of Figure 8), which shows the effect of removing additional catalog objects and scan artifacts from S by [E. Solano et al. \(2022\)](#). Across the western celestial hemisphere, SPF in the set R ($N = 5,399$) tend to hug the plane of the Galaxy, suggesting that some fraction of these objects may be uncataloged stars, including uncatalogued dwarf stars that were transiently flaring during the POSS1-E exposures. There is also a marked depletion north of the celestial equator in the western hemisphere when compared to the eastern hemisphere in both W and R (white dashed outline in Figure 8). In the case of R , SPF in the western hemisphere above the Galactic plane have been almost totally erased. Before using R to search for images of unidentified objects, the origin of these patterns in the spatial distribution should be investigated and understood.

4.5. Clusters of aligned SPFs

[B. Villarroel et al. \(2025c\)](#) also searched for clusters of up to five SPFs exhibiting statistically significant alignments: i.e., that are unlikely to result from a Poisson point process for populations of comparable size. These were called “candidate alignments” and were presented in Table 3 of that study. As already mentioned, there is no reason to expect that plate artifacts that give rise to SPFs should have a spatially uniform-random distribution (as if generated by a Poisson point process). We presented strong evidence that they are not uniform-random distributed, by highlighting SPFs in regions with clear linear boundaries (Section 4.3). In light of these observations, discovering clusters of aligned SPFs is not especially surprising. In this section, we focus on the nature of the specific SPFs that have been identified as belonging to the candidate linear clusters in Table 3 of [B. Villarroel et al. \(2025c\)](#).

At the start of Section 4 in [B. Villarroel et al. \(2025c\)](#), the authors write “We base our analysis on the catalog of 298,165 short duration transients presented in [Solano et al. \(2022\)](#), detected in red POSS1 plates with typical exposure times of 45–50 minutes.” This implies that the search for aligned SPFs made use of S ($N = 298,165$), which according to [E. Solano et al. \(2022\)](#) is 96.8% composed of features that reside within 5” of a catalog star (including what we have called set W). Indeed, as shown in our Table 2, we find that 8 of the 24 SPFs belonging to candidate linear clusters in Table 3 of [B. Villarroel et al. \(2025c\)](#) reside within 2” of an object in W (a subset of S), suggesting that these features represent one and the same object. [B. Villarroel et al. \(2025c\)](#) recomputed the astrometric positions of SPFs in Table 3 ([B. Villarroel](#)

Table 2. SPFs within quasilinear clusters reported in Table 3 of [B. Villarroel et al. \(2025c\)](#) with an angular separation (d_W) of less than 2” from an SPF in W . That is, 8 of 24 listed are probable matches to SPFs in W . Set W consists of SPFs whose celestial coordinates at the time of observation resided within 5” of a NeoWISE catalog object. RA and Dec. coordinates are reported for the J2000 reference frame.

Cluster	Object	RA [deg]	Dec. [deg]	d_W [as]
1	2	37.339083	28.616081	1.7
	3	37.340667	28.613636	1.8
4	3	321.198417	68.533033	0.7
	4	321.1655	68.525339	1.1
	6	321.016417	68.487322	0.8
5	3	289.190542	51.481122	1.8
	4	289.167208	51.453569	1.7
	5	289.167792	51.451747	1.7

[et al. 2025c](#)) with respect to positions originally reported for SPFs in W from [E. Solano et al. \(2022\)](#), which likely accounts for the $< 2''$ positional differences we see here. We have confirmed that 8 of 24 SPFs in Table 3 of [B. Villarroel et al. \(2025c\)](#) are located within 5” of a NeoWISE catalog object position (a 9th is $\sim 5.1''$ away). These members of set W were removed from S by [E. Solano et al. \(2022\)](#) when constructing R because they were not confidently distinguished from NeoWISE objects. For the same reason, [B. Villarroel et al. \(2025c\)](#) also removed W from S to construct the set V used in other analyses. No reason is given in [B. Villarroel et al. \(2025c\)](#) for reverting to set S to search for SPF alignments representing satellite glints.

We manually examined the SuperCosmos and DSS images of all SPFs in Table 3 of [B. Villarroel et al. \(2025c\)](#) and show two comparisons in Figure 9. We have noted a marked qualitative asymmetry of some of these SPFs, indicating the need for a quantitative morphological analysis. (A morphological analysis is also recommended by the presence of the anomalous shapes of some SPFs in R as shown in Figure 2.) In Figure 8 of [B. Villarroel et al. \(2025a\)](#), the lowermost member of the cluster of three SPFs (red arrows in part B of our Figure 9) is described as “slightly dubious in shape”. In our high-magnification view, this is clearly an asymmetrical feature. As an important reminder, the SPFs in S have not been aggressively filtered for a high degree of radial symmetry. These images also highlight two defects of the kind that can be removed by scan comparison, in this case appearing on the SuperCosmos scan and not the DSS scan (yellow arrows). These artifacts are also clearly identified in Figure 8 of [B. Villarroel](#)

et al. (2025c). Parts C and D of our Figure 9 show another SPF from an aligned cluster (object 3 in cluster 5 of Table 3 in B. Villarroel et al. (2025c)) that also exhibits clear elongation, although is possibly a pair of overlapping sources. An additional star-like SPF artifact appears in the lower right (yellow arrow).

5. FREQUENCY OF OCCURRENCE IN EARTH'S SHADOW

B. Villarroel et al. (2025c) have alleged there is a deficit of SPFs within the Earth's umbra, whose radius is roughly 8.5° at the altitude of geosynchronous orbits (GSO). This was reported as a $30 - 75\%$ reduction in the frequency of SPFs with respect to expectations, at levels of statistical significance ranging from 2.5σ to 22σ . The significance was calculated using Poisson uncertainties, which are appropriate for Poisson point processes: i.e., the authors have assumed that the background population of SPFs is spatially uniform-random. They have cited the reported deficit of SPFs in the shadow as evidence for the hypothesis that a significant fraction of SPFs represent objects reflecting sunlight in geosynchronous orbits. According to the authors, such objects are expected to produce point-like glints rather than along-track streaks during the POSS1-E 50 minute exposures. As mentioned earlier, they have acknowledged the existence of invalid detections in their dataset (e.g., plate artifacts), but have assumed that these would exhibit a uniform-random distribution that is superposed on the true distribution of non-astronomical light sources. In addition to the null statistical hypothesis just mentioned, this assumption is explicitly stated (e.g., see section 3 on "Predictions and Expectations" in B. Villarroel et al. (2025c): "Plate defects, by contrast, are expected to be randomly shaped and distributed").

Elsewhere, B. Villarroel et al. (2025c) acknowledges the overdensity of SPFs near plate edges without plotting, quantifying, or otherwise characterizing this effect. SPFs more than 2° away from plate centers were removed (i.e., to construct set V'' ; see Table 1) and the in-shadow SPF frequency analysis was repeated, still finding a significant deficit of SPFs in the shadow ($\sim 30\%$), although with marginal statistical significance owing to the smaller sample size (2.6σ). B. Villarroel et al. (2025c) acknowledged the increase in SPFs near plate edges as plate-related, without demonstrating that the processes that generates SPFs near the edges of plates do not also generate SPFs at the centers of plates.

To assess the reported deficit of SPFs in the Earth's shadow, we have simulated the shadowing of SPFs and plates. We have used the most aggressively-filtered data set, R , from which catalog objects and probable digitization artifacts have been removed. We have divided each plate into 30×30 cells of equal size, and then calculated the minimum distance of the center of each cell to the center of Earth's shadow using the `earthshadow` library (G. Nir 2024) used by B. Villarroel et al. (2025c), during each 50 minute exposure. Cells passing within 8.5° of the shadow center are considered to have been at least potentially "in shadow" at the altitude of geosynchronous orbits (as in B. Villarroel et al. (2025c), who also considered the smaller shadow at twice the GSO altitude). We have used this to estimate the total shadowed solid angle (in degrees), and we compared this to the total observed solid angle (i.e., the area of the sky covered by the POSS1-E survey in the northern celestial hemisphere). The ratio of these quantities (f_{exp}) is the fraction of the sky surveyed within the shadow in square degrees. We also computed the fraction of SPFs within shadow (f_{obs}) of the 4,866 that could be unambiguously assigned to a plate footprint. We found that $f_{\text{obs}} = 66/4866 = 1.36\%$ and $f_{\text{exp}} = 0.82\%$. For the most heavily filtered and aggressively vetted dataset, we did not find a deficit of SPFs in the shadow.

We found that just 10 plates overlap the shadow (consistent with the number reported in B. Villarroel et al. (2025c)). Their plate IDs are: 728, 070P, 070Q, 070S, 0810, 08L2, 08L9, 08RS, 08RV, and 090W. The plates with over 50% overlap by area are 728, 08L2, 08L9, 08RS, and 090W; plate 08L9 contains the largest number of in-shadow SPFs (36). These amount to just $\sim 1.5\%$ of the total number of plates which contained SPFs (reported as 635 for V in B. Villarroel et al. (2025c)). The footprints of these 10 plates have been plotted in Figure 8C on the map of number density of SPFs in R (see Section 4.4).

Based on the results in Section 4, the spatial distribution of SPFs is not uniform-random. We do not know the expected distribution of plate- and digitization-related artifacts, which depends on a host of poorly-characterized processes related to the manufacture and degradation of the photographic medium, and the scanning of plates. A highly nonrandom distribution of these artifacts could significantly affect the relative proportion measured in a tiny fraction of the sky, such as the area covered by Earth's shadow at geosynchronous altitudes. For example, consider the case where the distribution of SPFs is roughly uniform-random except that a handful of plates contains an enormous number of obvious plate artifacts: an example is Plate 090R with its 2,149 SPFs in W , nearly 20 times the average SPF count per plate. If the few plates with the overdensity happen to reside outside of the shadow, then the few shadowed plates will

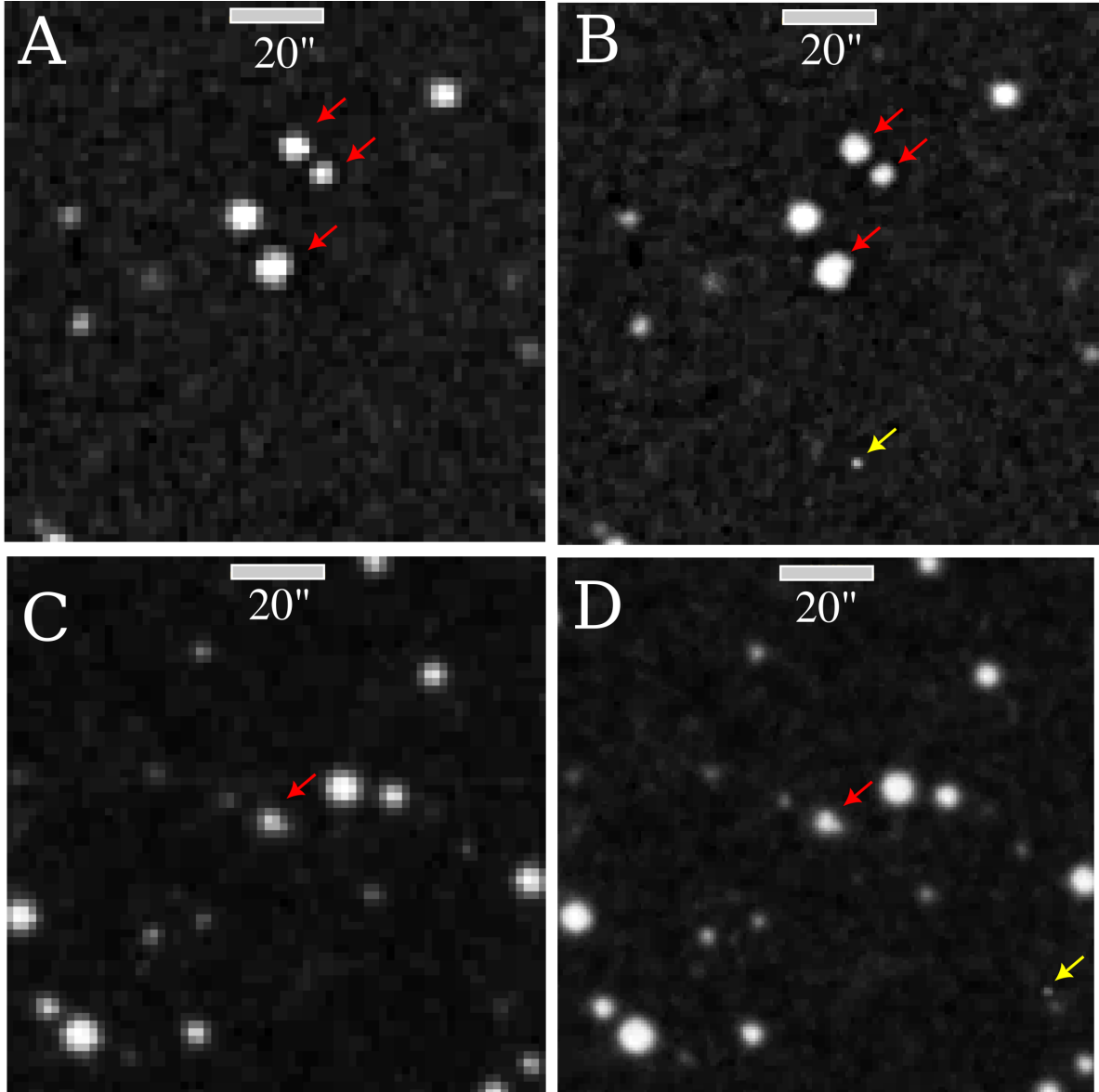


Figure 9. Magnified images of SPFs belonging to candidate linear clusters detailed in Table 3 of [B. Villarroel et al. \(2025c\)](#) (red arrows) and SPF scan artifacts present in SuperCosmos scans (B and D) and absent from DSS scans (A and C) of the same field (yellow arrows). The noticeable departure from circular symmetry in the case of multiple objects marked with red arrows suggests that S should be aggressively filtered to remove features without an extremely high degree of radial symmetry, as expected for the point source glints hypothesized in [B. Villarroel et al. \(2025c\)](#), in order to avoid likely artifacts.

contain fewer SPF s per square degree than the population as a whole.

Another important problem with the in-shadow frequency calculation is that set V was derived from S which, as we have seen, was determined by [E. Solano et al. \(2022\)](#) to consist primarily of objects that have not been distinguished from catalog stars and scan defects. At least 95% (i.e., $1 - N_R/N_V$) of SPF s in V were discarded by [E. Solano et al. \(2022\)](#) to produce the aggressively-vetted subset R (see Table 1). And yet, V was used instead of R to compute the in-shadow frequency of SPF s.

In summary, in order to fully understand the source of the reported deficit of shadowed SPF s in V , it is important to understand the variations in SPF number density at a wide range of scales—from the scale of individual plates as seen in Figures 4 through 7, to the scale of the entire sky as seen in Figure 8. Plate degradation and digitization, feature detection algorithms, as well as catalog filtering and post-processing, all may affect the number density of the shadowed regions while being unrelated to the shadow itself. For example, it is essential to understand the origin of features like the western hemisphere void that we noted in R (part B of Figure 8), and the vertical stripe-shaped void between roughly RA = 90° and RA = 105° (part C of Figure 8) that we have noted in W and R , and then to examine how shadowed plate footprints and relative SPF counts are affected.

6. TEMPORAL DISTRIBUTION AND ALLEGED CORRELATION WITH NUCLEAR TESTS

[S. Bruehl & B. Villarroel \(2025\)](#) sought to relate the timing of SPF s in V and the timing of nuclear weapons tests. They defined the time window of their study as spanning November 19, 1949 to April 28, 1957, inclusive. Of the 2,718 days in this period, “observed transients” (SPF s) were found on only 310 days according to [S. Bruehl & B. Villarroel \(2025\)](#). However, an examination of the POSS1-E plates set reveals that the 937 plate observations were conducted on a total of only 380 days, of which 368 days (906 plates) fall within this study time period. The analysis that follows brings the number of observation days in dataset V down to a maximum of 312. Based on W and R , it is also likely that nearly all of the POSS1-E plates sampled to construct V contained SPF s, suggesting that the reported correlation between SPF s and nuclear tests is almost entirely determined by the Palomar telescope observation schedule. We have plotted the dates of the nuclear tests, as well as the POSS1-E plate observation days (“plate days”), in Figure 10.

6.1. Replication study

[S. Bruehl & B. Villarroel \(2025\)](#) claimed there is a significant (Chi-Square = 6.94, $p = 0.008$) correlation between nuclear tests in the study time window and the occurrence of SPF s. Table 3 shows the results presented in Table 1 of [S. Bruehl & B. Villarroel \(2025\)](#) for dataset V . We attempted to replicate these results using the three sources cited in [S. Bruehl & B. Villarroel \(2025\)](#) (see Section 3) for nuclear test dates, and the publicly available SPF datasets R and W . (The full dataset used by [S. Bruehl & B. Villarroel \(2025\)](#) (V) was not publicly available at time of writing.) We find a slight count difference in nuclear test dates: [S. Bruehl & B. Villarroel \(2025\)](#) report 124 test dates while we account for 125 dates, likely due to differences in how we parsed the three sources of nuclear test dates.

Since the R (most vetted) and W (larger statistics) datasets do not include plate identification numbers or timestamps, we had to match every detection from these datasets to a POSS1-E plate and its associated timestamp using the method described in Section 4.1. We excluded SPF s from the datasets which have either no associated plate or ambiguous plate association using this method; this corresponds to about 10% of the SPF s in R and 12% in W . While there are discrepancies, both in the list of nuclear test dates and in the subset of SPF s that have unambiguous timestamps associated with them, these are trivial and do not change the outcome of the correlation analysis.

6.2. Normalization by the true observation window

SPF s are reported in the V dataset ([B. Villarroel et al. 2025c](#)) on 310 days out of the 2,718 days in their study period. [S. Bruehl & B. Villarroel \(2025\)](#) find that 255 of these 310 days occur outside any nuclear testing window and 54 days occur inside a nuclear testing window; the testing window is defined by [S. Bruehl & B. Villarroel \(2025\)](#) as a day of nuclear testing ± 1 day. In order to test for significant correlation between the detection of SPF s and the nuclear testing windows, [S. Bruehl & B. Villarroel \(2025\)](#) compared these numbers (255 days and 54 days, respectively) to the days with and without detected SPF s, that occur within the full time period of 2,718 days. In reality, the POSS1 survey did not record observations every single day out of this time period ([R. L. Minkowski & G. O. Abell 1963; STScI 2026](#)). There are plates available for only 380 days, of which 368 fall within the study period.

In addition, we argue that the conservative normalization of 368 days counted within the study period during which plates are available, can be further reduced if we account for the lack of SPF sampling in the southern

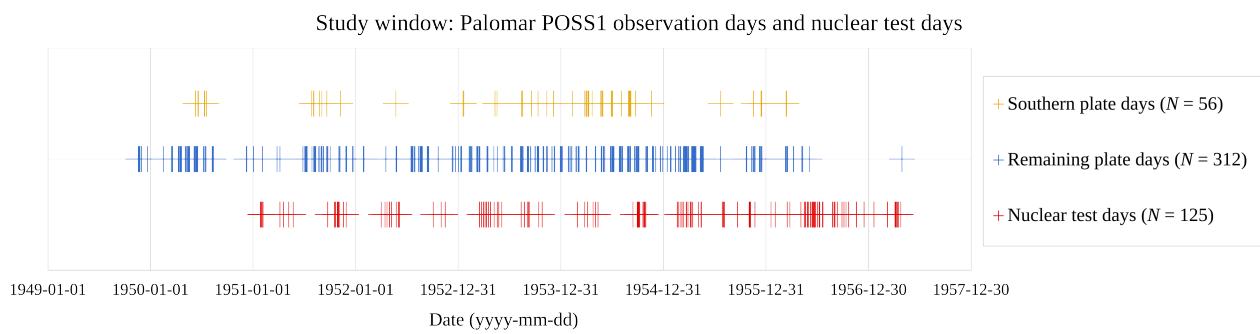


Figure 10. From top to bottom, plots of the observation dates (i) with POSS1-E plates solely residing completely in the southern celestial hemisphere; (ii) all remaining plate days (northern celestial hemisphere and/or overlapping the celestial equator); and (iii) the dates of nuclear test explosions.

hemisphere. The footprints of 31% of the 937 POSS1-E plates reside entirely in the southern celestial hemisphere without overlapping the celestial equator. But as explained in Section 3, the datasets R , W and V contain SPFs overwhelmingly located in the northern celestial hemisphere. Set W contains less than 0.1% of SPFs in the southern celestial hemisphere, while R contains 1.4% and V also contains 1.4% (see Section 3 and Appendix A). The southern hemisphere SPFs in these datasets reside overwhelmingly in equatorial plates that were acquired on the same day as at least one northern hemisphere plate, and so they do not contribute to the count of total unique observation days. This discrepancy between the northern versus southern hemisphere distribution of SPFs suggests that the plates whose footprints fully reside in the southern hemisphere were not sampled in search of SPFs for set A and its subsets (S , P , W , R , and V) (see Section 3 and Appendix A), and the corresponding southern hemisphere-only observation days should be removed from the total count of observation days (Figure 10).

Hence, for the R and W datasets, we can safely assume that the 56 days on which POSS1-E observations were taken exclusively in the southern celestial hemisphere during the study period are not relevant to this correlation analysis. Excluding these days, the maximum number of observation days with northern hemisphere POSS1-E plates (i.e., whose footprints reside completely within or overlap the northern hemisphere) falls from 368 days to 312 days. We find only 289 unique observation days represented in R and 307 in W after matching each of their SPFs to an unambiguous plate, which is very close to the 310 days reported in S. Bruehl & B. Villarroel (2025) for V . Thus, within the study time window, at least one SPF from W (respectively R) dataset was found on 98% (respectively 93%) of the days that the POSS1 survey imaged the northern sky. This suggests that SPFs are not a rare event, they occur on almost every observation day, even within the most filtered set R , and their occurrences are almost entirely dictated by the POSS1 observation schedule.

In the case of set V , if we use the conservative normalization of 368 days (including days observing only the southern hemisphere), SPFs were detected on 84% of the days that POSS1-E exposures were taken during the study period. Since the proportion of southern hemisphere SPFs in V is the same as in R and similar to W , it can be inferred that the southern hemisphere plates were not sampled to construct V , either. In that case, the fraction of POSS1 observation days on which SPFs were detected in V is 99%.

If we naively repeat in Table 3 the correlation test by replacing the 2,718 days of the full time period with the effective 312 observation days of the POSS1 survey, and using the publicly available, most vetted R dataset instead of V , the p-value for a correlation between SPF detection and nuclear testing window goes to $p = 0.1$, which is no longer significant, and the relative risk ratio goes to 1.07 (95% confidence interval: 1.02 - 1.13). The relative risk ratio here is defined as the conditional probability $\mathbb{P}(\text{SPF detection}|\text{Nuclear test}) = 98.1\%$ divided by the conditional probability $\mathbb{P}(\text{SPF detection}|\text{No nuclear test}) = 91.5\%$. A reasonable interpretation is that SPFs are 7% more likely to fall within a nuclear test window compared to outside of a nuclear test window (instead of 45% as claimed in (S. Bruehl & B. Villarroel 2025)).

6.3. Correlation between POSS1 observation schedule and nuclear test schedule

This approach is still not satisfactory because it ignores the correlation between nuclear test windows and the observation schedule of POSS1. If we compare the full 368 observation days of the POSS1 survey in the study time window and the days within a nuclear testing window, we find that 56 days overlap, which corresponds to 15% of the observation days. S. Bruehl & B. Villarroel (2025) report that 54 days match with both an SPF observation and a nuclear testing window. In other words, our analysis suggests that 96% of the claimed significant overlap between transient observations and nuclear testing windows simply stems from the chance overlap between the POSS1-E observation schedule and the presumably independent nuclear testing schedule.

We have repeated the correlation test, comparing the 2,718 days of the full time period with the 312 observation days of the POSS1 survey to estimate the degree of underlying correlation between the observation schedule and the nuclear test windows. The relative risk ratio is 1.35 (with a p-value of 0.03 and a 95% confidence interval: 1.03 - 1.78); in other words a POSS1 observation day is 35% more likely to fall within a nuclear test window compared to outside of a nuclear test window.

Overall, it is not surprising to find a correlation between days on which SPFs were recorded and nuclear test windows considering that (i) SPFs are reported by S. Bruehl & B. Villarroel (2025) on at least 84% (probably 99%) of the days on which the POSS1 survey was observing; and (ii) the POSS1 observation schedule has a non-negligible (35%) likelihood of falling within nuclear test windows compared to outside. Moreover, normalizing by the effective POSS1 observation days instead of the full time period significantly dilutes the significance

Source	S. Bruehl & B. Villarroel (2025)		This study			
Dataset used	<i>V</i>		<i>R</i>			
Normalization	All days in study time window(2,718)		All days in study time window (2,718)		Observation days relevant to the study (312)	
SPF observed?						
Within nuclear testing window?	No	Yes	No	Yes	No	Yes
No	2,116 (89.2%)	255 (10.8%)	2130 (89.9%)	238 (10.1%)	22 (8.5%)	238 (91.5%)
Yes	293 (84.4%)	54 (15.6%)	299 (85.4%)	51 (14.6%)	1 (1.9%)	51 (98.1%)

Table 3. Left table: reproduction of Table 1 from [S. Bruehl & B. Villarroel \(2025\)](#). Middle and right tables: our day counts obtained after properly normalizing by the observation window. We have used the most vetted dataset *R* instead of *V*. Due to smaller statistics overall, *R* contains only 290 days where SPFs were found as opposed to 310 days found by [S. Bruehl & B. Villarroel \(2025\)](#) in the *V* dataset. The nuclear testing window is defined in [S. Bruehl & B. Villarroel \(2025\)](#) as a day of nuclear testing ± 1 day. Percentages in parenthesis show the conditional probabilities of observing (or not observing) an SPF given the presence (or absence) of a nuclear test on that day. Observation days relevant to this study are the days on which plates are sampled (“plate days” in Figure 10) solely from the northern celestial hemisphere and/or overlapping the celestial equator.

of the statistical effect reported between SPF detection and nuclear testing. We speculate that the correlation may be due to seasonality, since both the timing of astronomical observations and nuclear testing rely on clear weather conditions, but further investigation would be required to fully explain it.

The observation that SPFs were observed on nearly all the days on which observations were acquired, also undercuts significance that has been assigned to the reported correlation between SPFs and UAP sighting reports in [S. Bruehl & B. Villarroel \(2025\)](#).

7. DISCUSSION

Research related to SETI and UAP is commonly concerned with searching for unusual signals against a background that is contaminated with artifacts and other sources of noise. For these fields to advance, it is essential that analyses and conclusions are preceded by rigorous data validation. This step is essential even in cases where it is extremely difficult. [E. Solano et al. \(2022\)](#) constructed the dataset R ($N = 5,399$) after removing objects that could not be readily distinguished from astronomical objects, plate artifacts, and scan artifacts. A logical next step is to determine whether any of these features represent an optical transient: that is, whether any originated from a light source in front of the telescope, with a corresponding optical path. The lack of data validation in [B. Villarroel et al. \(2025c\)](#) and [S. Bruehl & B. Villarroel \(2025\)](#) has led to the erroneous assumptions and reasoning, contradictions, and mistaken conclusions that we have described in this paper.

7.1. Analyzing unvalidated data

The most important problem with the [B. Villarroel et al. \(2025c\)](#) and [S. Bruehl & B. Villarroel \(2025\)](#) studies is that the dataset V and its subsets have not been validated in ways that are necessary for their use in a scientific study. In reference to the dataset V of “carefully selected transient samples,” the authors concede that “this sample has not been visually inspected. As such, it is expected to contain a substantial number of false positives, including clustered artifacts such as edge fingerprints or other plate defects that contaminate our sample.” The basic question of “what do the data points represent?” has not been answered. We have argued that this is absolutely required for anything of value to be extracted from these data.

We suggest that it is probably essential to perform detailed experiments to record optical flashes with a similar or identical instrument and optical medium to gain confidence that optical flash candidates can be distinguished from plate defects. Based on previous work

(see Section 2) this requires the identification of a robust set of criteria for microscopic evaluation of individual features in the emulsion of glass plates. A parallel task is to ensure that each optical flash candidate is not related to any known fast astronomical transient or other known sources of optical flashes (see for example [R. Hudec \(1993\)](#)). This work may benefit from a microscopic examination of known high-altitude satellite glints in photographic plates post-dating POSS1. In addition, it would be important to study the processes that tend to degrade and contaminate photographic plates, resulting in additional plate artifacts. As previously noted, a morphological analysis with a more stringent symmetry filter could be used to remove additional artifacts, in order to highlight a smaller subset of R that could serve as the focus of these investigations.

7.2. Importance of characterizing and addressing background variations

Before performing tests of statistical significance to understand the relationship to terrestrial shadowing, the null probability of alignments, and the correlation with nuclear tests, it is vital to examine and understand what the dataset contains: what its data points represent. If, as in the present case, the composition of the dataset is not known, the main sources of variation can at least be explored. A further essential step is to characterize and model these sources of variation (e.g., the overdensity in regions near the Galactic plane) and account for them *before* examining the relationship to other factors. In the present study, we have shown that the primary processes generating SPFs are very likely not optical transients; these processes should be modeled and addressed before assessing second-order effects and searching for rare events like optical transients.

In the present study, we have displayed the intra-plate distribution of SPFs, finding that SPFs increase in number density toward the plate edges in W and R . We have also shown other noteworthy patterns that occur in plates on an individual basis, including clusters far away from edges (see Figure 4). Without showing or modeling the intra-plate distribution of SPFs in V' to identify an appropriate remedy, [B. Villarroel et al. \(2025c\)](#) removed SPFs located near plate edges (resulting in V'') and repeated the estimate of the SPF number density in shadowed plates. The result of this analysis had marginal statistical significance and was not reported in the study abstract. The key significance of these patterns in number density, which clearly relate to plate geometry, is that they implicate a generative process related to the plates themselves. This process (e.g., the production of plate emulsion defects) may account for the overwhelm-

ing majority of SPF in V , whether in plate interiors or near edges, and which are therefore unlikely to be related to objects in the sky.

7.3. Expected spatial distribution of plate artifacts

[B. Villarroel et al. \(2025c\)](#) uses contradictory assumptions about the expected spatial distribution of defects, in some places assuming these cluster along edges, and in other places assuming the expected distribution to be “random” (e.g., see section 3 on “Predictions and Expectations” in [B. Villarroel et al. \(2025c\)](#): “Plate defects, by contrast, are expected to be randomly shaped and distributed”). Both cannot be true.

This is prominently revealed by the attention paid to statistical tests of significance, to illustrate a *nonrandom* distribution, such as a deficit of SPF in Earth’s shadow and SPF alignments. Since we do not understand in detail the processes that can generate plate artifacts, it is not clear that a random distribution is the correct null hypothesis. A templating process (see our Section 4.3) could produce plate artifacts exhibiting alignments; for example, the shape created by SPF in part A of Figure 4 has sharply-defined edges made from dense clusters of SPF. A relative deficit of SPF in a tiny fraction of the sky (e.g., the simulated terrestrial shadow at GSO covered just 1.5% of the sampled POSS1-E plates) could be entirely explained by excesses of SPF that may have occurred in plates strongly affected by degradation (see Section 4.1), or conversely by deficits arising from features like the large-scale voids visible in Figure 8 (see Section 4.4).

7.4. Inconsistent statements concerning data preparation

[B. Villarroel et al. \(2025c\)](#) contains statements about the extent to which V and its subsets were filtered to remove spurious detections and catalog objects, which are often inconsistent with each other or inconsistent with descriptions in [E. Solano et al. \(2022\)](#) about the preparation of the parent sets A and S . In Section 2 of [B. Villarroel et al. \(2025c\)](#), the authors write “we shall use carefully selected transient samples in Solano et al. (2022), which... have been matched to several modern surveys to remove variable stars, asteroids, and comets.” But V and its subsets are nowhere defined in [E. Solano et al. \(2022\)](#), which states that asteroids and variable stars were removed as part of the construction of R ($N = 5,399$), only after removing star-proximate SPF from S (see Table 1); this leaves a remainder of $N = 9,171$, which is clearly too small to be the source of V . The removal of “comets” is mentioned nowhere in [E. Solano et al. \(2022\)](#). These and other inconsistent

statements have made it impossible to accurately reconstruct the definitions of datasets. We have highlighted additional inconsistent remarks about the dataset V and its derivatives in Appendix A.

7.5. Circular reasoning and tautological claims

Circular or tautological reasoning involves assuming the conclusion of an argument as part of its premises. [B. Villarroel et al. \(2025c\)](#) and [S. Bruehl & B. Villarroel \(2025\)](#) make widespread use of the word “transient” to describe what we have termed “SPFs” (Selected POSS1 Features). The word “transient” implies that the features in question are in fact images of short-lived light sources, before this has been demonstrated. For example, consider this statement from page 2 of [B. Villarroel et al. \(2025c\)](#):

- “Clarifying the origin of these transient events is therefore not only of astrophysical interest but also of potential importance for one of the most enigmatic and consequential questions facing science today.”

This text uses the words “transient events” to refer to features on photographic plates, which the same study has elsewhere acknowledged may primarily consist of plate artifacts. This leading statement implicitly skips a critical unanswered question. This is akin to asking “is this feature a UFO or a plane?” without first establishing that it represents an optical flash that was emitted by an object in front of the telescope.

Using the *result* of an inferential analysis as an independently-demonstrated fact can also lead to circular reasoning. [B. Villarroel et al. \(2025c\)](#) invokes the inferred nonrandom distribution of SPF (deficit in the Earth’s shadow, sporadic alignments, correlation with timing of nuclear tests) as evidence for the validity of the data underpinning that analysis. The circularity of this argument is illustrated in Figure 11. That is, if the SPF are valid images and not plate artifacts, then the calculated deficit of SPF in the shadow and the positive temporal correlation with nuclear tests are leveraged to suggest that these represent images of real objects or events in outer space. But how do we know that the SPF are valid images? The answer from [B. Villarroel et al. \(2025c\)](#) appears to be, at least in part: because of a calculated deficit of SPF in the shadow and a positive temporal correlation with nuclear tests. This circular argument results from an analysis that appears to confirm a hypothesis (specific nonrandom distributions), used to explain the measurements *as well as* support their validity. We give two examples of this device from [B. Villarroel et al. \(2025c\)](#):

- “...authentic events may coexist on the same plate as numerous star-like defects, which makes it essential to apply independent diagnostics such as alignment statistics and Earth’s shadow tests.” (pg. 3)
- “Even if individual events remain uncertain, Bruehl & Villarroel (2025) shows statistically significant correlations between subsets of the transient sample in Solano et al. (2022) and historical nuclear activity and aerial anomalies. This alone contradicts the idea that the entire sample consists of plate defects.” (pg. 3)

As we have discussed in Section 6, the correlation between SPF and nuclear tests appears to be determined largely or entirely by the Palomar telescope observation schedule. This correlation may therefore be related to seasonal changes and other conditions that are favorable to both activities. Section 5 also showed that set R , the most aggressively vetted set of SPF, has no deficit of SPF in Earth’s shadow.

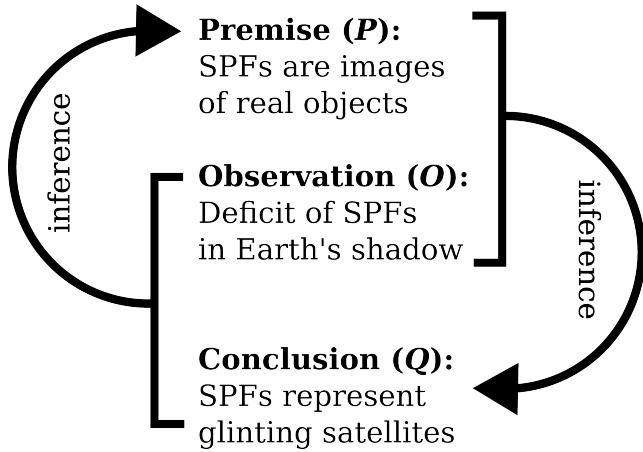


Figure 11. Illustration of an example of circular reasoning applied in [B. Villarroel et al. \(2025c\)](#), in which a premise and observation are used to justify a conclusion, while elsewhere the observation and conclusion are also used to justify confidence in the premise.

8. CONCLUSIONS

Searching telescopic observations from the pre-Sputnik era for unidentified luminous and reflecting objects is a novel approach to searching for the existence of technosignatures in proximity to Earth. It is vital, however, that these searches work from datasets that have been independently validated to represent true optical transients. In our critique of [B. Villarroel et al. \(2025c\)](#) and [S. Bruehl & B. Villarroel \(2025\)](#), we have pointed

out issues with replicability stemming from ambiguous definitions of datasets, as well as issues related to analyses and reported results, many of which arise from a lack of specific and comprehensive validation. In summary, we offer the following list of conclusions.

1. We conducted a review of optical transient searches in photographic plates, in the context of historical searches for the optical counterparts of Gamma Ray Bursts (GRBs). Following two decades of work, researchers were not able to make a confident identification; even tentative identification of optical flashes required close microscopic analysis, which [B. Villarroel et al. \(2025c\)](#) did not perform. This and preceding work ([B. Villarroel et al. 2021, 2022; E. Solano et al. 2022, 2024](#)) have not heeded the primary lessons from this literature. If robust criteria for identifying optical flashes in archival plates are eventually identified, this leaves the problem of how to rule out alternative sources of optical flashes such as astronomical fast transients and flashing lights on aircraft.
2. We have noted discrepancies between the definitions and uses of datasets of Selected POSS1-E Features (SPFs) in [E. Solano et al. \(2022\)](#) and [B. Villarroel et al. \(2025c\)](#). In searching for SPF that are not likely to be plate artifacts, digitization artifacts, or catalog objects, [E. Solano et al. \(2022\)](#) discarded 98.1% of dataset S ($N = 298,165$), leaving just 5,399 SPF in R . In spite of this, [B. Villarroel et al. \(2025c\)](#) analyzed the set S and subsets comprising roughly 35% of S (the subsets V ($N = 107,875$) and V' ($N = 106,339$)); [S. Bruehl & B. Villarroel \(2025\)](#) focused entirely on the set V . Based on [E. Solano et al. \(2022\)](#), R is the only subset of S that may contain genuinely unidentified features, and hence the only one that potentially contains the optical transients that are of interest for technosignature searches. But as mentioned, R itself requires validation by microscopic inspection of individual SPF ([J. Greiner et al. 1990](#)) if a robust set of criteria for identification of optical flashes can be established. If other datasets derived from [E. Solano et al. \(2022\)](#) are to be used for technosignature searches, then it is essential to explain why the filtering in [E. Solano et al. \(2022\)](#) was overzealous.
3. The SPF in subsets of S examined here exhibit distinctive spatial distributions in some plates that are clearly related to the plate boundaries and the celestial coordinate system (Figures 4, 6, and 7),

implicating generative processes that relate to the manufacture, storage, handling, and digitization of photographic plates, or the subsequent processing of the datasets. We have discussed the possible templating of SPF placements via zones of contact with other objects and surfaces, or preferential exposure of some regions to degradational processes. We have also noted that the increase in SPFs with distance from plate centers is qualitatively consistent with the results of experimental studies of endemic plate emulsion defects (J. Greiner et al. 1987).

4. The on-sky distribution of SPFs in W reveals a window of right ascension in which there is a marked deficit of SPFs not present in the POSS1-derived M dataset of likely celestial objects. We have also highlighted a void above the Galactic plane in the western celestial hemisphere in set R . We have pointed out the importance of characterizing and modeling sources of spatial variation at all scales in order to identify sources of variation influencing the in-shadow frequency and which are unrelated to the shadow itself. We find no significant in-shadow deficit of SPFs from the aggressively-filtered set R .
5. After normalizing properly by the number of observation days (the days on which plates were exposed, rather than the total span of time in the study window), the correlation reported in S. Bruehl & B. Villarroel (2025) between SPFs and nuclear tests can be explained by the incidental correlation between nuclear tests and the POSS1-E observation schedule. This correlation may, in turn, depend on factors that influence both of these activities, such as seasonal effects.
6. We have also highlighted examples of tautological claims and circular reasoning. Of special note is an argument invoking the consequences of explanatory hypotheses (i.e., an expected deficit of SPFs in the Earth's shadow) to provide justifica-

tion for confidence in the validity of measurements (i.e., that the SPFs represent images of real objects in space).

In summary, our study suggests that before proceeding further with the research program described in B. Villarroel et al. (2025c) and S. Bruehl & B. Villarroel (2025), far more work is needed to clearly define, understand, and validate the datasets under scrutiny. This work has been helpful, however, as motivating the contemporary search for technosignatures near Earth using specially-designed instrumentation, such as telescope arrays for triangulating the positions and characterizing the kinematics of anomalous interplanetary objects B. Villarroel (2024); B. Villarroel et al. (2025b). Although in some ways more complicated owing to the abundance of human spacecraft in orbit around Earth, this direction can avoid some of the challenges and pitfalls plaguing searches in historical photographic plates, as exemplified by GRB research after 1996.

ACKNOWLEDGMENTS

WW received a copy of V in July 2025 while collaborating on a manuscript that was published as B. Villarroel et al. (2025c) in late September 2025. When voluntarily withdrawing from this paper in July, WW raised early concerns regarding the spatial distribution of SPFs with the lead author (BV). The authors of B. Villarroel et al. (2025c) stated that “Data will be shared on reasonable request to the corresponding author,” presumably in reference to S or V . In the late fall of 2025, coauthors KK and LD (of this study) independently requested copies of these datasets, and were told they are not yet available. Because we have not obtained permission to publish analyses of V , we have used and reported here only on the publicly available datasets R and W . We are grateful to Doug Buettner, Tejin Cai, Mike Cifone, Eric Keto, Matthew Szenher, and Matthew Szydagis for helpful comments.

APPENDIX

A. AMBIGUITIES IN DATASET DEFINITIONS

As previously mentioned, the origins and reported sizes of V (used in S. Bruehl & B. Villarroel (2025)) and its subsets V' and V'' , used for key calculations in B. Villarroel et al. (2025c), are inconsistent or conflated in B. Villarroel et al. (2025c). We have listed some of these inconsistent statements here:

- From B. Villarroel et al. (2025c), pg 15: “We use the transient candidates from E. Solano et al. (2022), but with the additional requirement that they have no counterparts within 5'' in Gaia, Pan-STARRS and NeoWise.” The

initial candidate selection pool described in [E. Solano et al. \(2022\)](#), which we have called S , already did not included SPF near Gaia or Pan-STARRS objects ([E. Solano et al. 2022](#)). In any case, removing NeoWISE from S is consistent with our definition of set P in Table 1 (i.e., $S - W$ or $A - (a_0 \cup W)$), which has an expected size of $N = 126,412$.

- From [B. Villarroel et al. \(2025c\)](#), pg 15: “we restrict our analysis to objects in the northern hemisphere (decl. $> 0^\circ$). This yields a sample of 106,339 transients, which we use for our study” and later in the same section: “in our actual transient data set, only 349/107,875...” where 107,875 is clearly the total size of the set. We have taken this latter estimate to be the size of V and the former to be size of V' . These differ by 1.4%, consistent with the proportion of southern hemisphere SPFs in R .
- From [B. Villarroel et al. \(2025c\)](#), pg 3: “we shall use carefully selected transient samples in [Solano et al. \(2022\)](#), which average 167 transients per plate” and later “The transient sample is based on 635 unique photographic plates”, where $167 \times 635 = 106,045 \approx 106,399$.
- From [S. Bruehl & B. Villarroel \(2025\)](#), pg 6: “initial transient dataset consisted of a list of 107,875 transients”.
- From [B. Villarroel et al. \(2025c\)](#), pg 15: “We apply the published methodology and statistical framework to a published sample of POSS-I transients from [Solano et al. \(2022\)](#)”. As discussed, the only datasets that have been published from [E. Solano et al. \(2022\)](#) are R and W . The sets S , V , and V' used in [B. Villarroel et al. \(2025c\)](#) and [S. Bruehl & B. Villarroel \(2025\)](#) have not been published.

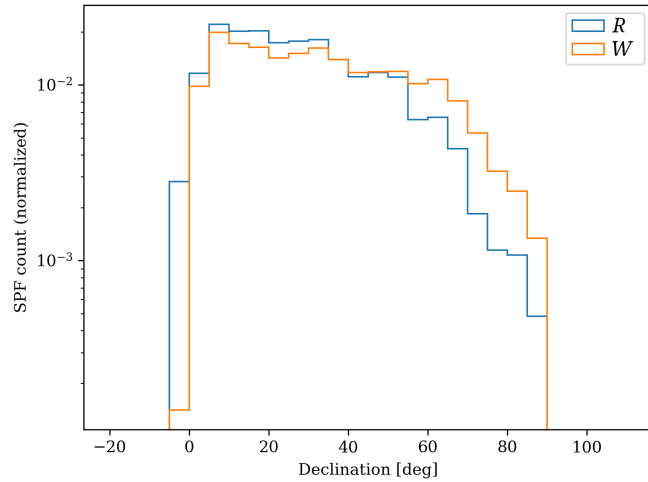


Figure 12. Histogram of the SPF counts as a function of declination in datasets R and W , suggesting that SPFs in the parent dataset (S) and its other derivatives (e.g., V) were overwhelmingly sampled from plates whose footprints reside entirely within or that overlap the northern celestial hemisphere. This was important for (i) understanding how the parent set was sampled, since this hemispherical bias is not mentioned in [E. Solano et al. \(2022\)](#); (ii) verifying that we have correctly inferred the size of set V (i.e., it has the same proportion of SPFs in the southern celestial hemisphere as R), and (iii) for identifying all dates on which observations were acquired, which is vital for assessing the correlation between SPF observations and nuclear tests in Section 6. The decrease in SPFs approaching the north pole is an effect of geometry (i.e., where there is less area per degree of declination).

Although set V is attributed to [E. Solano et al. \(2022\)](#), none of these definitions and reported sizes are consistent with the definitions and sizes of datasets defined in that earlier study. [E. Solano et al. \(2022\)](#) also did not report removing southern hemisphere SPFs or sampling in the southern hemisphere. The histogram of SPF counts as a function of declination for sets R and W is shown in appendix Figure 12, illustrating a deficit of sampling from the southern hemisphere plates. The proportion of SPFs in the southern celestial hemisphere is 1.4% in the case of set R

and 0.07% in the case of set W . Based on the reported sizes inferred for V ($N = 107,875$) and V' ($N = 106,399$), the proportion of southern-hemisphere SPF in V is 1.4%, consistent with the proportion in R .

REFERENCES

Ailleris, P. 2011, *Acta Astronautica*, 68, 2

Ailleris, P. 2024, *Limina-The Journal of UAP Studies*, 1, 11

Bruehl, S., & Villarroel, B. 2025, *Scientific Reports*, 15, 34125

Cabanela, J. E., Humphreys, R. M., Aldering, G., et al. 2003, *Publications of the Astronomical Society of the Pacific*, 115, 837

Chambers, K. C., Magnier, E. A., Metcalfe, N., et al. 2019, *The Pan-STARRS1 Surveys*, <https://arxiv.org/abs/1612.05560>

CHERCA. 2025, Centre for Health Effects of Radiological and Chemical Agents Tests conducted by Great Britain,

Clark, P. J., & Evans, F. C. 1954, *Ecology*, 35, 445

Dominé, L., Biswas, A., Cloete, R., et al. 2025, *Sensors* (Basel, Switzerland), 25, 783

Fishman, G. J., & Meegan, C. A. 1995, *Annual Review of Astronomy and Astrophysics*, 33, 415

Greiner, J. 1992, *Astronomy and Astrophysics* (ISSN 0004-6361), vol. 264, no. 1, p. 121-126., 264, 121

Greiner, J., Flohrer, J., Wenzel, W., & Lehmann, T. 1987, *Astrophysics and space science*, 138, 155

Greiner, J., & Moskalenko, E. 1994, *Astronomy and Astrophysics* (ISSN 0004-6361), vol. 283, no. 2, p. 693-697, 283, 693

Greiner, J., Wenzel, W., & Degel, W. 1990, *Astronomy and Astrophysics* (ISSN 0004-6361), vol. 234, no. 1-2, Aug. 1990, p. 251-261., 234, 251

Grindlay, J., Wright, E., & McCrosky, R. 1974, *Astrophysical Journal*, vol. 192, Sept. 15, 1974, pt. 2, p. L113, L114. NASA-supported research., 192, L113

Hambly, N., & Blair, A. 2024, *RAS Techniques and Instruments*, 3, 73

Hambly, N. C., MacGillivray, H. T., Read, M. A., et al. 2001, *Monthly Notices of the Royal Astronomical Society*, 326, 1279

Haqq-Misra, J., & Kopparapu, R. K. 2012, *Acta Astronautica*, 72, 15

Hudec, R. 1993, *Astrophysical Letters and Communications*, Vol. 28, p. 359, 28, 359

Hudec, R., Dedoch, A., Pravec, P., & Borovicka, J. 1994, *Astronomy and Astrophysics* (ISSN 0004-6361), vol. 284, no. 3, p. 839-852, 284, 839

Hynek, J. A. 1966, *Science*, 154, 329

Kayal, H. 2022, in *Extraterrestrial Intelligence: Academic and Societal Implications*, ed. J. Andresen & O. Torres (Cambridge Scholars Publishing), 87-111

Knuth, K. H., Ailleris, P., Agrama, H. A., et al. 2025, *Progress in Aerospace Sciences*, 101097

Lingam, M., Haqq-Misra, J., Wright, J. T., et al. 2023, *The Astrophysical Journal*, 943, 27

Loeb, A. A., & Laukien, F. H. 2023, *Journal of Astronomical Instrumentation*, 12, 2340003

Mainzer, A., Bauer, J., Grav, T., et al. 2011, *The Astrophysical Journal*, 731, 53

McDonald, J. E. 1972, in *UFOs: A Scientific Debate* (The Norton Library), 52-122

McNamara, B. J., & Harrison, T. E. 1998, *Nature*, 396, 233

Minkowski, R. L., & Abell, G. O. 1963, in *Basic Astronomical Data: Stars and Stellar Systems*, ed. K. A. Strand, 481

Morgan, D. 1995, in *IAU Colloq. 148: The Future Utilisation of Schmidt Telescopes*, Vol. 84, 137

NASA. 2023, <https://science.nasa.gov/uap/#hds-sidebar-nav-2>

Nir, G. 2024, *Earthshadow: Python Tools for Astronomical Shadow-Tracking*, <https://github.com/guynir42/earthshadow>

NNSS. 2023, Nevada National Security Site Tests conducted by the United States,

Nolan, G. P., Vallee, J. F., Jiang, S., & Lemke, L. G. 2022, *Progress in Aerospace Sciences*, 128, 100788, doi: <https://doi.org/10.1016/j.paerosci.2021.100788>

Pennington, R. L., Humphreys, R. M., Odewahn, S. C., Zumach, W., & Thurmes, P. M. 1993, *Publications of the Astronomical Society of the Pacific*, 105, 521

Schaefer, B. E. 1981, *Nature*, 294, 722

Schaefer, B. E. 1990, *Astrophysical Journal*, Part 1 (ISSN 0004-637X), vol. 364, Dec. 1, 1990, p. 590-600., 364, 590

Schaefer, B. E. 1994, in *AIP Conference Proceedings* No. 1, American Institute of Physics, 382-391

Schaefer, B. E., Barber, M., Brooks, J. J., et al. 1987, *Astrophysical Journal*, Part 1 (ISSN 0004-637X), vol. 320, Sept. 1, 1987, p. 398-404., 320, 398

Shostak, S. 2020, *International Journal of Astrobiology*, 19, 456

Solano, E., Marcy, G. W., Villarroel, B., et al. 2024, *Monthly Notices of the Royal Astronomical Society*, 527, 6312

Solano, E., Villarroel, B., & Rodrigo, C. 2022, Monthly Notices of the Royal Astronomical Society, 515, 1380

STScI. 2026, Survey Plate list,,
<https://gsss.stsci.edu/skysurveys/SurveyPlateList.txt>

Szydagis, M., Knuth, K. H., Kugelsky, B., & Levy, C. 2025, Progress in Aerospace Sciences, 101099

Teodorani, M. 2004, Journal of Scientific Exploration, 18, 217

Vallenari, A., Brown, A. G., Prusti, T., et al. 2023, Astronomy & Astrophysics, 674, A1

Varady, M., & Hudec, R. 1992, Astronomy and Astrophysics (ISSN 0004-6361), vol. 261, no. 1, p. 365-371., 261, 365

Villarroel, B. 2024, in LPI Contributions, Vol. 3068, LPI Contributions, 2004

Villarroel, B., Mattsson, L., Guergouri, H., et al. 2022, Acta Astronautica, 194, 106,
 doi: <https://doi.org/10.1016/j.actaastro.2022.01.039>

Villarroel, B., Solano, E., & Marcy, G. W. 2025a, arXiv preprint arXiv:2507.15896

Villarroel, B., Watters, W. A., Streblyanska, A., et al. 2025b, Monthly Notices of the Royal Astronomical Society, staf1158

Villarroel, B., Marcy, G. W., Geier, S., et al. 2021, Scientific Reports, 11, 1

Villarroel, B., Solano, E., Guergouri, H., et al. 2025c, Publications of the Astronomical Society of the Pacific, 137, 104504

Vrba, F. J. 1996, in AIP Conference Proceedings No. 1, American Institute of Physics, 565–574

Vrba, F. J., Hartmann, D. H., & Jennings, M. C. 1995, The Astrophysical Journal

Watters, W. A., Loeb, A., Laukien, F., et al. 2023, Journal of Astronomical Instrumentation, 12, 2340006

Wikipedia. 2025, Tests conducted by the Soviet Union, Zytkow, A. N. 1990, Astrophysical Journal, Part 1 (ISSN 0004-637X), vol. 359, Aug. 10, 1990, p. 138-154., 359, 138